Clay Minerals, (2014) **49**, 247–275

Regional illitization in bentonite beds from the East Slovak Basin based on isotopic characteristics (K-Ar, $\delta^{18}O$ and δD) of illite-type nanoparticles

N. CLAUER[1,*], M. HONTY[2], A. E. FALLICK[3], V. ŠUCHA[4] AND A. AUBERT[1]

[1] *Laboratoire d'Hydrologie et de Géochimie de Strasbourg (CNRS-UdS), 1 Rue Blessig, 67084 Strasbourg, France,* [2] *SCK-CEN, Health, Environment and Safety Institute, Boeretang 200, 2400 Mol, Belgium,* [3] *Scottish Universities Environmental Research Centre, East Kilbride, Glasgow G75 0QF, UK, and* [4] *Faculty of Natural Sciences, Comenius University, Mlynská Dolina, 842 15 Bratislava, Slovak Republic*

(*Received 28 May 2012; revised 18 December 2012; Editor: Harry Shaw*)

ABSTRACT: Nanometre-sized illite-type crystals extracted from mixed-layer illite-smectite of cored bentonite beds from the East Slovak Basin were studied to investigate timing, duration and physical/chemical conditions of their nucleation and growth. The study includes application of the results to an evaluation of the regional extent of illitization. Close to salt-bearing formations, the nanometric particles underwent a more intense illitization, of identical duration, but with changing oxygen and hydrogen isotope characteristics of the parental brines.

A comparison of the stratigraphic ages of the bentonite beds with the K-Ar ages of the authigenic crystals shows that illitization started during the Middle-Miocene Serravalian (Lower Sarmatian) subsidence that lasted from 17 to 11.5 Ma. Duration of illitization was bracketed between 14.5 and 9.0 Ma, with further episodes until recently at 0 Ma, depending on the geographic location of the host beds. The calculated subsidence rate varies from less than 300 m/Ma to more than 500 m/Ma and the thermal gradient ranges from ~60ºC/km to less than 50ºC/km. The K-Ar ages of the nanometric illite point to either short-duration illitization when the onset was soon after sedimentation, or long-duration when the onset was significantly later after sedimentation. The illite $\delta^{18}O$ varies little with increasing crystal size, whereas the δD changes significantly. In most samples the crystallization temperature determined by different criteria did not change significantly during crystal growth, but the oxygen and hydrogen isotopic compositions of the interacting fluids varied depending on sample location, immediate environment, timing and duration of illitization.

The stable isotope composition of illite in bentonite beds with reduced fluid-rock ratios gives insight into the fluid-temperature regime of sedimentary basins through identifying local processes rather than wide-scale ones. Illitization is episodic with variable duration along different crystallization pathways, and to various extents in low-porosity, low-permeability bentonite beds. Depending on local conditions, illitization may vary even within apparently homogeneous beds. This contrasts with the situation for porous aquifers having large-scale fluid connectivity.

KEYWORDS: illitization, illite-type nanoparticles, nucleation/growth, East Slovak Basin, bentonite beds, K-Ar dating, $^{18}O/^{16}O$ and D/H characterization.

* E-mail: nclauer@unistra.fr
DOI: 10.1180/claymin.2014.049.2.07

Since the mid-1960s, illitization has been widely used as a tracer for reconstructing the evolution of sedimentary basins. Its application has been

explored along varied lines of investigation using textural-mineralogical indicators (e.g. Dunoyer de Segonzac, 1970; Hower *et al.*, 1976; Velde, 1985; Jennings & Thompson, 1986; Šucha *et al.*, 1993), combined organic-inorganic controls (Kübler, 1997; Clauer *et al.*, 1999), and isotopic dating and characterization (e.g. review in Clauer & Chaudhuri, 1995). It is generally considered to act as a continuous process mainly driven by temperature increase and interaction with interstitial fluids during progressive burial. Recent isotope studies of nanometre-sized illite-type "fundamental" particles in the sense of Nadeau *et al.* (1984) that consist of the illite layers from mixed layered illite-smectite structures (labeled I-S hereafter) provided new potential for evaluation of the duration and mechanism of burial-induced illitization, especially in bentonite beds of young sedimentary basins (Clauer *et al.*, 1997; Środoń *et al.*, 2002; Honty *et al.*, 2004; Środoń *et al.*, 2006). These nanometre-sized particles represent the smallest illite crystals technically separable with sizes as small as ~0.02 μm in the *ab* crystal plane and 0.002 μm in thickness; they grow progressively depending on the immediate environmental conditions. The direct interest in studying such small particles is in their size, which allows consideration of them as representative of the nucleating and subsequently growing crystallites. The reason for preferentially selecting bentonite beds from the East Slovak Basin as the host rocks in this reconstruction lies in the fact that these rocks are almost always devoid of detrital particles, which often bias the isotopic data (e.g. Clauer & Chaudhuri, 1995 and references therein; Clauer *et al.*, 1997).

Mathematical simulations of the relative abundances of detrital and authigenic components and the theoretical age of each represent plausible alternatives to the difficult technical challenge of separating authigenic from detrital particles. Mossmann (1991) was the first to report on such a model, followed by Środoń (1999). Lerman *et al.* (2007) evaluated a different approach by taking into account the fact that the detrital components alter with the authigenic ones when progressively buried, and therefore simulated the global behaviour of K and radiogenic ^{40}Ar of the sized mixtures. Recently, Szczerba & Środoń (2009) elaborated again on the acquisition of the ages of each illite-type component of the mixtures on the basis of mineralogical criteria, but discarding the natural alteration of the K-Ar system. Clauer & Lerman (2009) evaluated a kinetic approach to the gain and loss rates of K and radiogenic ^{40}Ar from detrital/authigenic mixtures relative to burial depth by following the progressively changing K-Ar system of both components relative to increasing depth. In fact, modelling K-Ar results of detrital/authigenic mixtures does not improve the knowledge of the illitization process itself, its extension at a basin scale or its duration. Different models are presently available to explain theoretically illitization, along dissolution-precipitation or solid-state alteration processes (e.g. Altaner & Ylagan, 1997), but such models are not very helpful either for evaluation of the duration of the mechanism as the isotopic ages are often biased by the occurrence of detrital minerals, which has been reported in many publications (e.g. Aronson & Hower, 1976; Burley & Flisch, 1989; Ehrenberg & Nadeau, 1989; Glassman *et al.*, 1989a,b; Peacor, 1992; Clauer & Chaudhuri, 1996; Clauer *et al.*, 1999). Alternatively, XRD profile modelling of illite-smectite mixed layers provides new promising insights into the illitization process (McCarty *et al.*, 2008) if such pure crystals can be isolated and analysed by isotopic means. The prospect of studying high-purity authigenic nanometre-sized illite crystals becomes therefore of great interest and prime importance.

Despite a few successful studies (e.g. Elliott *et al.*, 1991), generally applicable models are still lacking for the determination of duration and extent of illitization at basin scales, because these models are considered to depend mainly on the reliability of the time-temperature estimations in each specific basin, which in turn are expected to vary from basin to basin (e.g. Środoń & Eberl 1984). In sedimentary or volcanic ashy units at basin-wide scales, variable degrees of illitization may depend on the location and depth of the studied material, the changing impact of the chemical composition and temperature of the interacting fluids, and the thermal gradient and sedimentation rate. These aspects are essential for understanding the regional impact of the diagenetic evolution of clay material; they will be addressed here by combining K-Ar, and oxygen and hydrogen isotopic determinations of nanometre-size illite-type particles separated from I-S of well identified beds within the East Slovak Basin (western Carpathians). One of the expected goals is the creation of a regional record of illitization in units of the same rock facies, widely dispersed spatially, and of different depositional ages.

https://doi.org/10.1180/claymin.2014.049.2.07 Published online by Cambridge University Press

ISOTOPE RECORDS OF NANOMETRIC ILLITE CRYSTALS

On the basis of K-Ar, Rb-Sr and stable isotope data of nanometre- to micrometre-sized illite crystals from bentonite beds of sedimentary basins (Clauer *et al.*, 1997; Środoń *et al.*, 2002, 2006; Honty *et al.*, 2004), Clauer (2006) published a preliminary conceptual model for the behaviour of K-Ar and $\delta^{18}O$ characteristics of such nucleating and growing particles during progressive burial. Based on available analytical data, the model envisages different reaction rates and durations, also taking into consideration variable temperature increases and impacts of the fluid chemistry as influenced by the water/rock ratio.

Crystal growth depends on temperature, thermal-kinetic parameters and accessibility of the interstitial fluids to the particles in the sedimentary environment. For instance, nucleating particles that stop growing and remain small theoretically yield the oldest K-Ar ages in the particle-size distribution. Conversely, during crystal growth that proceeded intermittently rather than continuously, the smallest nanometre-sized crystals provide potentially younger K-Ar data than the associated coarser micrometre-sized particles because they nucleated when the earlier (and therefore coarser) crystals were growing and accumulating K and radiogenic ^{40}Ar. Therefore, K-Ar dating of nanometric particles from any bentonite I-S does not systematically provide unequivocally meaningful K-Ar ages that decrease when crystal size increases, as particles can potentially nucleate intermittently depending on local parameters, or be of successive origins and agglomerate into coarser sizes during fraction separation. In any case, "fundamental" nano-particles are most appropriate for reconstructing the history of bentonite beds, because the illite (and smectite) crystals are well defined; they are not affected by surface sorption and particle agglomeration, and their thickness distribution shapes conform to crystal growth theory (Eberl *et al.*, 2011). In addition, it is of importance, as we are dealing with K-Ar ages, to recall that these nanometric particles do not leak any radiogenic ^{40}Ar due to their particle size, as the smallest particles are often older than the coarser ones (e.g. Clauer *et al.*, 1997), which is of crucial importance for the exercise attempted here. This means that different size fractions of a sample can integrate particles of the same or similar mineral types but of variable ages, resulting from episodic and variable K supply. Such varied mineral types cannot be distinguished by traditional analytical procedures such as X-ray diffraction (XRD) or chemical analysis, although they might be so now with the XRD profile modelling mentioned above. In addition, K-Ar ages are also able to record information about the crystal-growth mechanism and reaction rate(s). For instance, the crystal growth rate may or may not have remained constant over time (fig. 3 of Clauer, 2006) with the mode of the K-Ar ages located either: (1) towards the middle of the theoretical time span of illitization when the rate was about constant; or (2) close to the beginning of the theoretical time span when the rate decreased or was interrupted; or (3) towards the end of the time span when the rate progressively increased. In summary, the K-Ar ages of bentonite illite-type nanoparticles are able to record the complicated illitization history that could have occurred in these strata by showing constant or varied growth rates, and one or successive nucleation/growth steps. If such scenarios occur in individual bentonite beds of a given stratigraphic age, the interpretation will be necessarily complicated, raising questions about the sample preparation and analysis, but also and more importantly about how to decipher the complex evolution of the whole sedimentary basin.

While electron microscope observations and X-ray diffraction measurements of nanometre-sized "fundamental" particles are informative about the physical aspects of particle growth, the $\delta^{18}O$ values of the separates can provide information about the conditions of nucleation and growth, especially about the chemical conditions of the fluid-particle interactions (fig. 4 of Clauer, 2006). A decrease of $\delta^{18}O$ from fine to coarse particles suggests either an increase in temperature, a change in the $\delta^{18}O$ of the interactive fluid, and/or a variable water/rock ratio during growth, whereas an increase in $\delta^{18}O$ implies the opposite. No information on hydrogen isotopic results of fundamental particles is yet available, to the best of our knowledge.

For completeness, it might be recalled that the label "fundamental" corresponds to extremely small crystals and aggregates that were obtained following a specific sample preparation and particle separation presented below. The term "fundamental" has no connotation other than the particles are of nanometre thickness. To avoid any

https://doi.org/10.1180/claymin.2014.049.2.07 Published online by Cambridge University Press

unnecessary rhetorical debate about the meaning of "fundamental" whilst accepting the concept and definition of Nadeau *et al.* (1984), the term nanometric will be adopted hereafter, although only partly appropriate because it refers only to the thickness of the particles in nanometres, whereas their width can be in micrometres.

GEOLOGICAL SETTING

The western Carpathians belong to a young orogen related to the eastern Alps in the west and to the eastern Carpathians in the east. They are divided into the neo-Alpine accretionary prism consisting of flysch nappes that thrust over the foredeep, and the consolidated palaeo-Alpine and meso-Alpine cratons; these two major units are separated by the tectonic suture of the Pieniny Klippen belt (Kováč *et al.*, 1997). One of the main driving mechanisms of the neo-Alpine geodynamic evolution of the eastern Carpathians was the subduction of the Flysch Belt basement (or foredeep) under the overriding plate (Royden, 1993; Tomek & Hall, 1993) that generated high geothermal gradients.

Most of the central region of the western Carpathians consists of thick Tertiary sedimentary and volcanic sequences that relate to the Pannonian back-arc basin system. The samples selected for the present study come from bentonite beds of the East Slovak Basin that were encountered in several boreholes (Fig. 1). The area of interest is the northwestern volcano-sedimentary basin of the Transcarpathian depression. Its development was controlled by the collision of the Carpathian orogen with the North European platform, and later by crustal extension and thermal subsidence in the Pannonian Basin. These processes changed from a compressive tectonic regime into an extensional regime, inducing palaeogeographic modifications during basin evolution. The basin is classified as a complex back-arc basin (Kováč *et al.*, 1995) with an asymmetrical Neogene infilling in both the longitudinal and perpendicular cross sections, and with steep fault scarps on its NE and SE margins. Based on a study by Rudinec (1990), the East Slovak Basin forms an asymmetric sedimentary foreland basin (Fig. 2) with a steeper ESE flank than the opposite flank and no major structural

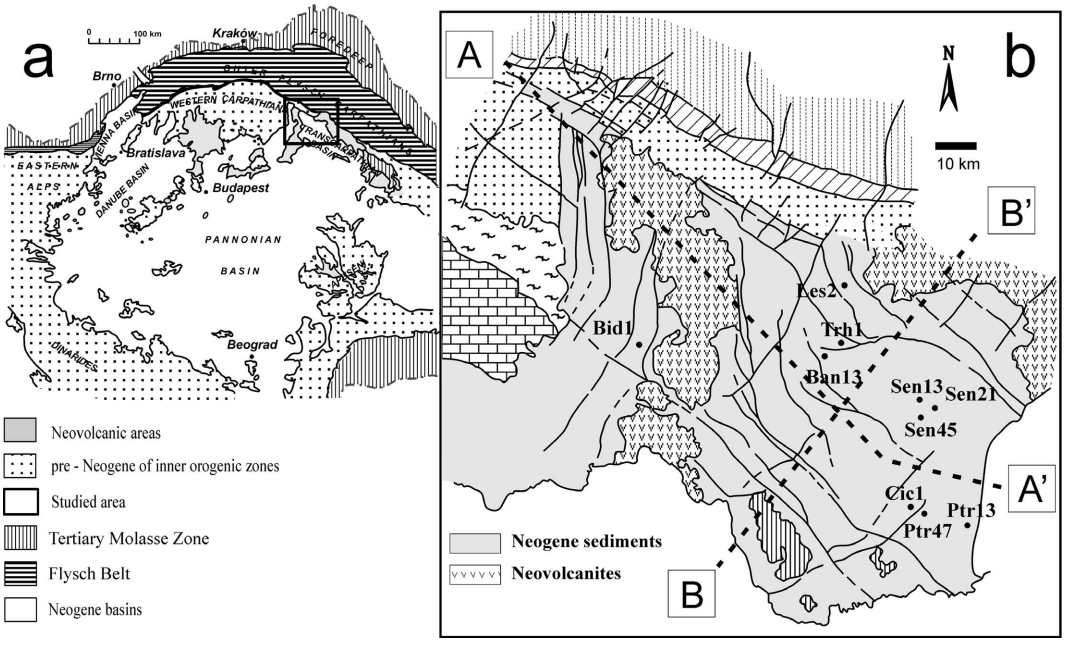

FIG. 1. (a) Location of the East Slovak Basin in the Pannonian system of Neogene basins (after Kováč *et al.*, 1995), and (b) Enlargement of the square of map (a) with the location of the studied boreholes in the basin. The longitudinal and transversal traverses of the basin shown in Fig. 2 are outlined by the lines A–A′ and B–B′, respectively (after Honty *et al.*, 2004).

https://doi.org/10.1180/claymin.2014.049.2.07 Published online by Cambridge University Press

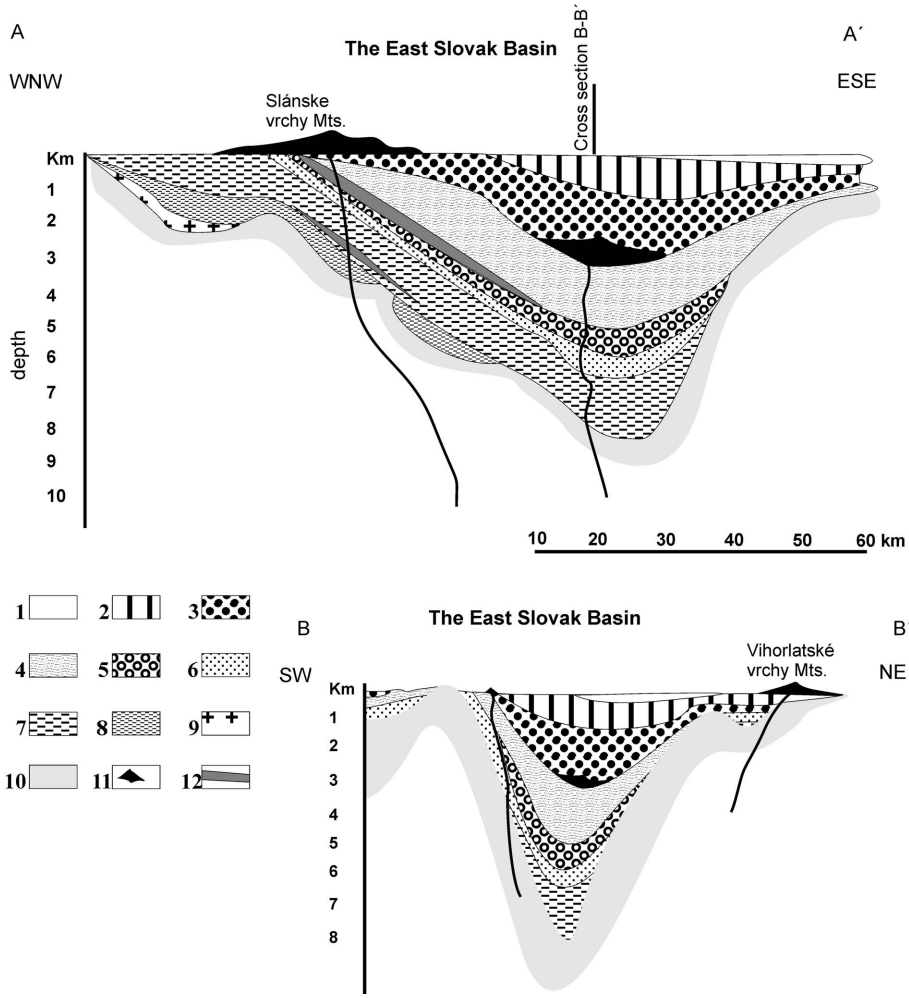

FIG. 2. Longitudinal and perpendicular traverses of the East Slovak Basin (after Honty *et al.*, 2004). Their locations are materialized by the lines A–A′ and B–B′ in Fig. 1. The numbered boxes correspond respectively to: 1 = Pliocene; 2 = Pannonian to Pontian; 3 = Sarmatian; 4 = Upper Badenian; 5 = Middle Badenian; 6 = Lower Badenian; 7 = Carpathian; 8 = Eggenburgian; 9 = Egerian; 10 = pre-Neogene basement; 11 = Neogene volcanics; 12 = salts.

features except some volcanic pipes. The perpendicular cross-section also shows a compressive infilling.

The Neogene sedimentary sequence attains a maximum thickness of 8–9 km. Except for one location in the south-centre of the basin, the studied bentonite units are located to the northeast and east of the basin. The samples come from beds that were deposited between the Middle Miocene Burdigalian (Lower Badenian) and the Middle Miocene Serravalian (Lower Sarmatian), from 17.0 to 11.5 Ma. The basin infill comprises a number of sequences deposited on a continental or transitional crust that shallow upward (Soták *et al.*, 1993). The buried andesite to rhyolite stratovolcano in the southeastern basin (Kováč *et al.*, 1995) was penetrated by the Cicarovce-1 well (Fig. 1). The volcanic sequences pass laterally into detrital sediments via numerous parallel to sub-parallel lava flows and pyroclastic layers.

The burial and thermal history of the East Slovak Basin was simulated using the *PetroMod ID*

https://doi.org/10.1180/claymin.2014.049.2.07 Published online by Cambridge University Press

software (Poelchau *et al.*, 1997; Honty *et al.*, 2004). The calculations include heat transfer during burial, compaction and thermal maturation of organic matter (with the EasyRo % software) based on the kinetic equations of Sweeney & Burnham (1990). To reconstruct the burial and thermal evolution of some of the sampled sequences, the model was calibrated with vitrinite reflectance data (Rr %) and present-day temperatures (Král *et al.*, 1985), as well as the heat-flow history, such as for the Senné profile (Fig. 3; see also Clauer *et al.*, 1997, and Honty *et al.*, 2004).

Three main periods of rapid tectonic subsidence were reported on the basis of back-stripping modelling of selected wells (Baráth *et al.*, 1997). Episodes of rapid subsidence were identified during the Lower Miocene Burdigalian (Carpathian, from 17.5 to 16.5 Ma), the Middle Miocene Langhian (Middle Badenian, from 15.5 to 14.5 Ma) and the Middle Miocene Serravallian (Lower Sarmatian, from 12.5 to 11.5 Ma) times, all separated by slow-subsidence periods. That from the Pannonian to the Quaternary (11.5 Ma to present) is characterized by a very slow tectonic subsidence, with a reconstruction that suggests a late uplift stage in some parts of the basin (Baráth *et al.*, 1997). The features of importance for the present study are: (1) the occurrence of acidic and calc-alkaline pyroclastic units that make up 20–30 vol.% of the sedimentary sequence (Vaas *et al.*, 1988); (2) a high heat flow related to the volcano-orogenic activity (Q = 82–113 $mW.m^{-2}$) inducing temperatures of ~210ºC at 4000 m depth (Král *et al.*, 1985); and (3) a thermal history of the basin allowing correlation of the degree of illitization with other palaeotemperature indicators.

MATERIALS AND METHODS

The bentonite units are generally visible in the cores as thin (centimetric to decimetric), altered, tuffitic beds intercalated in claystones or shales. Due to their limited thickness, no mineralogical or age zonation was observed in the beds, as was the case in the 2.5 m thick bentonite bed of the Disturbed Bed from Montana (Clauer *et al.*, 1997; McCarty *et al.*, 2009). Some of these beds are characterized by high Na contents explained by a long lasting interaction with hypersaline Badenian brines that originated in salt deposits (Magyar & Očovský, 1981). This salinity represents the principal difference, together with enhanced illitization, between the salt-bearing and salt-free material studied here as identified in Table 1 (Honty *et al.*, 2004). Brackish waters, which were not mixed with the saline brines, were recognized in the Upper Badenian and Lower Sarmatian (Michalíček, 1965, 1970).

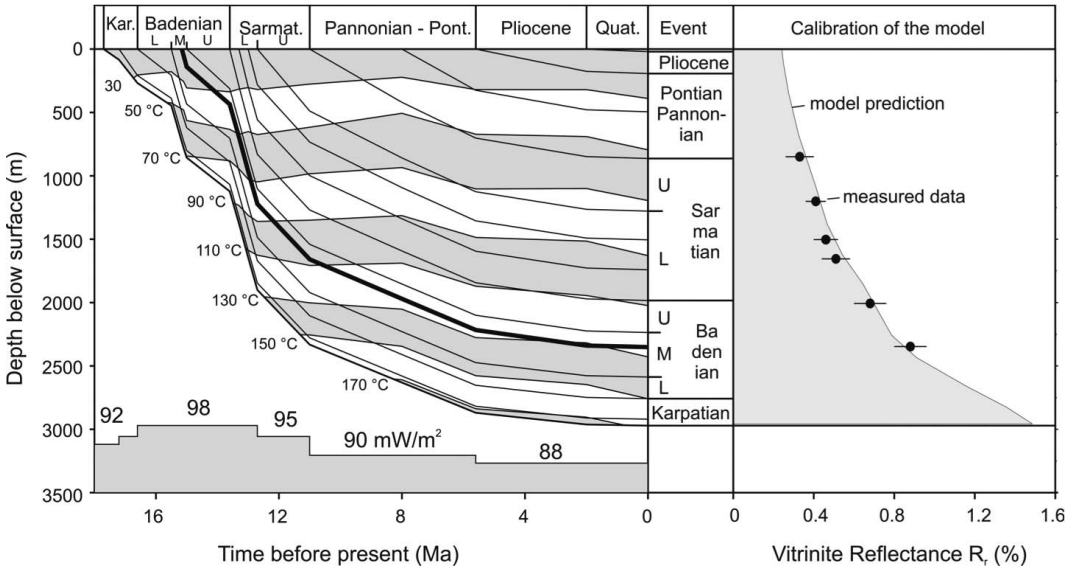

FIG. 3. Burial and thermal evolution of the Senné-45 well calibrated by the vitrinite reflectance data to the right. The bentonite bed is in bold (after Honty *et al.*, 2004).

https://doi.org/10.1180/claymin.2014.049.2.07 Published online by Cambridge University Press

TABLE 1. Identification, stratigraphic age, burial depth and expandability (in %S) of the studied samples.

Sample identification (<2 μm)	Sample IDs	Stratigraphic age (Ma)	Burial depth (m)	Measured temperature (ºC)	S_{XRD} (%)	I-S ordering
Salt-free samples						
Cicarovce 1/11	Cic1/11	Lower Sarmatian (12.5–11.5)	1614	97	90	R = 0
Cicarovce 1/12	Cic1/12	Lower Sarmatian (12.5–11.5)	1703	n.d.	30	R = 1/R = 3
Cicarovce 1/15	Cic1/15	Lower Sarmatian (12.5–11.5)	2002	116	28	R = 1/R = 3
Cicarovce 1/18	Cic1/18	Lower Sarmatian (12.5–11.5)	2296	131	51	R = 0
Cicarovce 1/20	Cic1/20	Lower Sarmatian (12.5–11.5)	2495	n.d.	45	
Trhoviste 1/37	Trh1	L. Badenian-U. Carpathian (17–15.5)	3015	165	18	
Salt-bearing samples						
Banovce 13/12	Ban13	Lower Badenian (16.5–15.5)	3313	n.d.	5	
Bidovce 1 3/1	Bid1 3/1	Lower Badenian (16.5–15.5)	1557	n.d.	70	R = 0
Bidovce 1 3/3	Bid1 3/3	Lower Badenian (16.5–15.5)	1565	n.d.	70	R = 0
Lesné 2 1A/3	Les2	Lower Badenian (16.5–15.5)	1046–1051	n.d.	0	–
Ptruksa 47 9/7	Ptr47	Upper Badenian (14.5–13.5)	2106–2115	n.d.	25	R = 1/R = 3
Ptruksa 13 14	Ptr13	Upper Badenian (14.5–13.5)	2095–2103	115	13	R = 1/R = 3
Senné 13 5A	Sen13	Middle Badenian (15.5–14.5)	2402	132	15	R = 1/R = 3
Senné 21 4/1	Sen21	Middle Badenian (15.5–14.5)	2311	134	10	R = 1/R = 3
Senné 45 1/5	Sen45	Middle Badenian (15.5–14.5)	2350	n.d.	15	

n.d.: not determined

The I-S mineral fraction was extracted from well identified bentonite beds of ten boreholes drilled into the East Slovak Basin, to the north of the Pannonian Basin (Fig. 1a,b). Most samples preserved features typical of the rhyolitic and andesitic protoliths, such as phenocrysts of corroded quartz, biotite, zoned feldspar and volcanic glass. The collected bentonite beds are from approximately 955 to 2402 m depth and their I-S contains from 90 to 0% smectite layers (Table 1; Honty *et al.*, 2004). The depths given for each set of samples are considered to be close to the maximum burial as no significant subsidence or uplift has been documented in the entire basin after ash deposition.

The whole-rock samples were gently crushed for 1–2 min, sieved and disaggregated in deionized water using an ultrasonic bath. The crushing periods were intentionally kept short to avoid over-crushing, but some of the isolated micrometric fine fractions could have resulted from this procedure. Nevertheless, we assume that the nanometric fractions did not originate in this way, as they would require a delamination of the particle interlayers. The slurries were treated with Na acetate buffer, Na dithionite and hydrogen peroxide (Jackson, 1975) to remove all of the soluble mineral phases and organic matter from the matrix; it is appropriate to recall here that such treatments do not alter the K-Ar isotopic system of the I-S (Clauer *et al.*, 1993). The <2 μm size fraction of each sample was then separated by sedimentation in distilled water following Stokes law, and the <0.2 μm fraction was collected by centrifugation. These <0.2 μm fractions were then diluted to a concentration of 1 g/40 L, in order to ensure an "infinite" osmotic swelling (Środoń *et al.*, 1992) and were further separated into smaller (<0.02, 0.02–0.05 and 0.05–0.1 μm) sub-fractions by continuous flow ultra-centrifugation. These finest fractions that correspond to the illite layers from initial I-S were then collected by flocculating the suspensions with NaCl and by removing the excess electrolyte by repeated centrifugation and dialysis. XRD patterns were obtained from oriented <2 and <0.2 μm fractions air-dried and treated with ethylene-glycol, and from random whole-rock powders.

The XRD patterns were determined on oriented air-dried (AD) and ethylene-glycolated (EG) specimens on an XRD diffractometer equipped with a graphite monochromator, using Cu-*K*α radiation, a 2–50º 2θ range, a 0.02º 2θ step size and a 5 s per step count time. The expandability was determined by the peak-position method described by Środoń (1980). The weighted mean thickness of the crystals was also calculated according to the Bertaut-Warren-Averbach (BWA) theory (Eberl *et al.*, 1998a), in addition to the routine XRD analysis of the different size fractions for mineral identification. The parameters α (mean of the natural logarithms of the thicknesses) and β^2 (variance of the natural logarithms of the thicknesses) were then deduced from crystal thickness distribution.

The K-Ar determinations were made using a procedure following that of Bonhomme *et al.* (1975). Potassium was measured by flame spectrophotometry on aliquots dried at 110ºC, with a reproducibility of ±1.5% based on repetitive determinations of the two standard powders B-EN and GL-O. For Ar analyses, the samples were preheated under vacuum at 80ºC for at least 12 h to reduce the amount of atmospheric Ar adsorbed on the mineral surfaces during sample preparation, separation and handling. The results were calibrated by repetitive analysis of the GL-O standard that averaged $24.73 \pm 0.30 \times 10^{-6}$ cm^3/g STP (2σ) of radiogenic ^{40}Ar during the course of the study. Also measured periodically, the $^{40}Ar/^{36}Ar$ ratio of atmospheric Ar averaged 287.2 during the same period. The reference values for these two standards are at $24.85 \pm 0.24 \times 10^{-6}$ cm^3/g for the amount of radiogenic ^{40}Ar in the standard (Odin *et al.*, 1982), and 295.5 for the atmospheric $^{40}Ar/^{36}Ar$ ratio (Nier, 1950). Internally consistent and close to the theoretical values, the measured calibration data were considered not to require discrimination corrections to the individual determinations. As the determined amounts of radiogenic ^{40}Ar were expected to be small due to limited content of K_2O and young stratigraphic ages, the "blank" of the extraction line and the mass spectrometer was measured before each Ar determination. The ^{40}Ar content of this blank was found to be systematically below 1×10^{-8} cm^3, which is significantly below the contents of radiogenic ^{40}Ar, implying analytically reliable determinations even for the very small contents, allowing us to disregard the amounts of blank ^{40}Ar in the age calculations. The accepted decay constants were used for the age calculations (Steiger & Jäger, 1977) and the overall error was evaluated to be routinely better than ±2% (2σ); in some specific cases it was higher due to both low K contents and young ages (Table 2).

https://doi.org/10.1180/claymin.2014.049.2.07 Published online by Cambridge University Press

TABLE 2. K-Ar, $\delta^{18}O$ and δD data of the studied grain size fractions. n.d. stands for not determined.

Sample identification (size in μm)	Sample IDs	K_2O (%)	Rad. Ar (%)	Rad. ^{40}Ar (10^{-6} cm^3/g)	Age (Ma (+/−2σ)	H_2O^+ (μmol/mg)	$\delta^{18}O$ ‰ (V-SMOW)	δD‰ (V-SMOW)
Salt-free samples								
Cicarovce 1/11 (2–1)	Cic1/11	1.35	2.0	0.33	7.6 (0.5)	3.81	13.44	–61
Cicarovce 1/11 (1–0.2)		1.17	1.5	0.30	8.0 (1.1)	3.79	14.31	–46
Cicarovce 1/11 (0.2–0.05)		0.96	0.4	0.03	1.0 (0.6)	3.61	14.58	–45
Cicarovce 1/11 (0.05–0.02)		1.04	0.0	0	0	n.d.	15.06	n.d.
Cicarovce 1/11 (<0.02)		0.79	0.1	0.02	0.6 (0.8)	2.99	14.89	–100
Cicarovce 1/12 (0.2–0.05)	Cic1/12	3.44	14.3	0.72	6.4 (0.3)			
Cicarovce 1/12 (0.05–0.02)		4.61	29.0	2.39	16.0 (0.4)			
Cicarovce 1/12 (<0.02)		3.77	14.8	1.16	9.5 (0.4)			
Cicarovce 1/15 (2–1)	Cic1/15	2.51	9.7	0.35	4.3 (0.2)	3.65	11.78	–49
Cicarovce 1/15 (1–0.2)		4.82	6.6	0.73	4.7 (0.1)	3.48	11.66	–58
Cicarovce 1/15 (0.2–0.05)		5.56	3.0	0.83	4.6 (0.1)	3.71 (3.68)	12.21	–38
Cicarovce 1/15 (0.05–0.02)		5.57	14.6	0.77	4.3 (0.1)	3.69	12.17	–77
Cicarovce 1/15 (<0.02)		5.52	3.7	0.56	3.2 (0.1)	3.64	12.55	–74
Cicarovce 1/18 (<0.2)	Cic1/18	2.53	10.9	0.61	7.5 (0.3)			
Cicarovce 1/18 (0.2–0.05)		2.57	11.4	0.59	7.1 (0.3)			
Cicarovce 1/18 (0.05–0.02)		2.52	2.5	0.21	2.6 (0.9)			
Cicarovce 1/18 (<0.02)		2.32	4.1	0.55	7.4 (0.4)			
Salt–bearing samples								
Bidovce 1 3/1 (<0.2)	Bid1 3/1	2.09	3.0	0.63	9.4 (6.2)			
Bidovce 1 3/1 (0.2–0.05)		2.66	4.4	0.88	10.2 (0.5)			
Bidovce 1 3/1 (0.05–0.02)		2.18	2.6	0.44	6.3 (0.4)			
Bidovce 1 3/1 (<0.02)		1.52	2.3	0.36	7.4 (0.9)			
Bidovce 1 3/3 (<0.2)	Bid1 3/3	2.30	3.8	0.62	8.3 (4.2)			
Bidovce 1 3/3 (0.2–0.05)		3.23	5.1	1.06	10.1 (0.4)			
Bidovce 1 3/3 (0.05–0.02)		2.35	3.6	0.73	9.7 (0.5)			
Bidovce 1 3/3 (<0.02)		1.61	3.6	0.55	10.6 (0.6)			
Lesné 2 1A/3 (2–1)	Les2	5.82	22.0	1.97	10.5 (0.2)	3.73	15.69	–29
Lesné 2 1A/3 (1–0.2)		7.65	53.4	2.86	11.5 (0.2)	3.23	14.92	–46
Lesné 2 1A/3 (0.2–0.05)		7.52	64.3	2.83	11.6 (0.2)	3.39	14.80	–74
Lesné 2 1A/3 (0.05–0.02)		6.89	28.2	2.30	10.3 (0.3)	2.70	16.31	– 47 (–51)
Lesné 2 1A/3 (<0.02)		6.29	20.3	2.10	10.3 (0.3)	2.27	16.59	–121
Ptruksa 47 9/7 (2−1)	Ptr47	2.86	35.1	1.14	12.3 (0.5)			
Ptruksa 47 9/7 (1−0.2)		5.42	21.7	2.17	12.3 (0.3)			
Ptruksa 47 9/7 (0.2−0.05)		5.88	39.3	1.94	10.2 (0.2)			
Ptruksa 47 9/7 (0.05−0.02)		5.49	9.5	1.05	5.9 (0.4)			
Ptruksa 47 9/7 (<0.02)		5.81	11.7	1.68	9.0 (0.2)			

For the stable hydrogen isotope analyses, the samples were vacuum-degassed at 200°C overnight to remove the interlayer and absorbed surface water in a previously outgassed Pt crucible. The crucible was then placed inside a quartz extraction chamber attached to the vacuum line and evacuated. Dehydroxylation was accomplished by radiofrequency induction heating of the crucible at 1200°C. The water released was converted to H_2 by reaction with Cr at 800°C (Bigeleisen *et al.*, 1952; Donnelly *et al.*, 2000) in a multiple-pass system. The H_2 yield was measured manometrically and δD determined on a gas-source mass spectrometer calibrated via water and mineral standards. Using these techniques, the NBS30 biotite standard gave δD = −65‰ (V-SMOW) with an analytical precision of ±6‰ (2σ) (see Fallick *et al.*, 1993).

The oxygen isotope composition of the clay minerals was determined by laser fluorination (Macaulay *et al.*, 2000) using the Borthwick & Harmon (1982) ClF_3 modifications to Clayton & Mayeda's (1963) method. The precision was ±0.6‰ (2σ) and the NBS28 quartz standard yielded a $\delta^{18}O$ of 9.6‰ (V-SMOW). All clay isotope data are reported in parts per mil (‰) relative to the V-SMOW standard. As indicated in Tables 2 and 3, duplicates display acceptable internal reproducibility.

RESULTS

The XRD results

The XRD study of the powdered whole rocks confirmed the occurrence of non-clay mineral phases such as quartz, plagioclase and K-feldspars that were observed on a macroscopic scale, together with dolomite in sample Ptr47 and halite in sample Les2. Mixed with dominant I-S, these non-clay mineral phases are not "detrital" *ss*, such as in sandstones or shales, as the host rocks derive from volcanic ash during irregular and multiple volcanic eruptions (Honty *et al.*, 2004). Their preservation in marine sediments depends on the contest between ash fallout and background sedimentation (Kolata *et al.*, 1996). XRD analysis of the oriented <2 μm slurries which showed that I-S is the most abundant clay mineral in the selected bentonite units; in some cases it was the sole mineral phase detected. The I-S formed after deposition during diagenesis induced by progressive temperature increase in the presence of interstitial fluids. The second most dominant clay

TABLE 3. K-Ar data from previously studied bentonite samples of the East Slovak Basin.

Sample identification (size in μm)	Sample IDs	Stratigraphic unit	K_2O (%)	rad. Ar (%)	rad. ^{40}Ar (10^{-6} cm^3/g)	Age Ma (+/-2σ)	H_2O^+ (μmol/mg)	$\delta^{18}O$ ‰ (V-SMOW)	δD ‰ (V-SMOW)
Salt-free samples[(1)]									
Cicarovce 1/20 (2−0.5)	Cic1/20	Lower Sarmatian (12.5−11.5 Ma)	2.37	8.8	0.60	7.8 (1.8)			
Cicarovce 1/20 (0.3−1)			4.07	8.2	0.67	5.1 (1.2)			
Cicarovce 1/20 (0.1−X)			3.88	7.0	0.47	3.7 (1.1)			
Cicarovce 1/20 (X−Y)			4.18	6.0	0.52	3.8 (2.0)			
Cicarovce 1/20 (<Y)			2.32	6.1	0.56	7.2 (2.4)			
Trhoviste 1/37 (2−0.5)	Trh1	Lower Badenian to	5.55	45.0	1.77	9.9 (0.4)			
Trhoviste 1/37 (0.5−0.3)		Upper Carpathian (17−15.5 Ma)	7.36	49.3	2.68	11.3 (0.5)			
Trhoviste 1/37 (0.1−X)			7.76	39.8	2.56	10.2 (0.5)			
Trhoviste 1/37 (X−Y)			7.14	41.5	1.83	7.9 (0.4)			
Trhoviste 1/37 (<Y)			6.63	48.7	1.74	8.1 (0.3)			

Salt-bearing samples[2]									
Banovce 13/12 (2−0.2)	Ban13	Lower Badenian (16.5−15.5 Ma)	2.17	43.4	1.02	14.5 (0.9)			
Banovce 13/12 (0.2−0.02)			5.92	32.9	2.39	12.5 (0.8)			
Banovce 13/12 (<0.02)			6.32	44.8	2.56	12.5 (0.6)			
Senné 45 1/5 (2−0.2)	Sen45	Middle Badenian (15.5−14.5 Ma)	5.54	43.6	1.33	7.5 (0.4)			
Senné 45 1/5 (0.2−0.1)			6.95	28.2	1.74	7.8 (0.6)			
Senné 45 1/5 (<0.02)			6.96	16.6	2.07	9.2 (1.1)			
Senné 13 5A (2−1)	Sen13	Middle Badenian (15.5−14.5 Ma)	4.33	11.3	1.45	10.3 (0.4)	3.55	21.90 (22.15)	–96
Senné 13 5A (1−0.2)			5.95	14.9	1.57	8.2 (0.2)	2.55 (2.55)	19.45	–40(–39)
Senné 13 5A (0.2−0.05)			6.93	14.5	1.14	5.1 (0.1)	3.21	18.39	–58
Senné 13 5A (0.05−0.02)			6.86	7.8	0.66	3.0 (0.1)	3.61	17.61	–94
Senné 13 5A (<0.02)			7.94	4.2	0.56	2.2 (0.1)	3.17	18.67	–87
Senné 21 4/1 (2−1)	Sen21	Middle Badenian (15.5−14.5 Ma)	2.87	16.8	1.03	11.1 (0.4)			
Senné 21 4/1 (1−0.2)			5.54	28.8	1.24	6.9 (0.1)			
Senné 21 4/1 (0.2−0.05)			7.98	16.2	1.03	4.0 (0.1)			
Senné 21 4/1 (0.05−0.02)			6.78	20.9	1.21	5.5 (0.1)			
Senné 21 4/1 (<0.02)			6.67	12.0	0.95	4.4 (0.1)			
Ptruksa 13 14 (2−1)	Ptr13	Upper Badenian (14.5−13 .5 Ma)	1.77	15.2	0.61	10.6 (0.4)	2.08	16.61	–46
Ptruksa 13 14 (1−0.2)			4.17	29.2	1.09	8.1 (0.2)	2.79	15.68	–43
Ptruksa 13 14 (0.2−0.05)			6.90	31.5	1.78	8.0 (0.1)	3.43	14.77	–85
Ptruksa 13 14 (0.05−0.02)			6.92	22.9	1.71	7.6 (0.2)	2.94	15.49	–87
Ptruksa 13 14 (<0.02)			6.94	16.8	1.61	7.2 (0.1)	3.29	15.10	–42

[1] from Clauer *et al.*, 1997; [2] from Honty *et al.*, 2004.

The H_2O^+ contents and the $\delta^{18}O$ and δD values of this table were obtained during the present study, while the K-Ar data are from previous publications. The letters X and Y stand for grain sizes that were difficult to determine at the time of the publication (see Clauer *et al.*, 1997). The H_2O^+ contents and the $\delta^{18}O$ and δD values in brackets correspond to duplicate analyses.

mineral is kaolinite, while chlorite was detected with a dioctahedral illite in one sample.

The <2 μm fractions were examined for the expandability of the I-S (%S = percentage of smectite in the I-S) to evaluate indirectly the degree of illitization (Table 1; Fig. 4). The changing illitization grade is supported by low K_2O contents in the least illitized fractions (e.g. Bid1 3/1, Bid1 3/3 and Cic 1/11), and high contents in the most illitized fractions (Honty *et al.*, 2008). Between 1050 and 3015 m depth, which corresponds to a present-day burial temperature from about 50 to 130ºC, the expandability varies between 90 and 0%S, with an $R = 0$ ordering for I-S when >40%S and an $R>1$ to $R>3$ ordering for I-S when <40%S. Intense illitization was recorded between 1703 and 2002 m in several bentonite units of Cicarovce 1 well above the buried strato-volcano. A typical indicator of illitization is the shift of the first basal I-S XRD reflection from 5º (2θ) to higher 2θ angles and an attendant decrease of expandability that declined from 90%S in sample Cic1/11

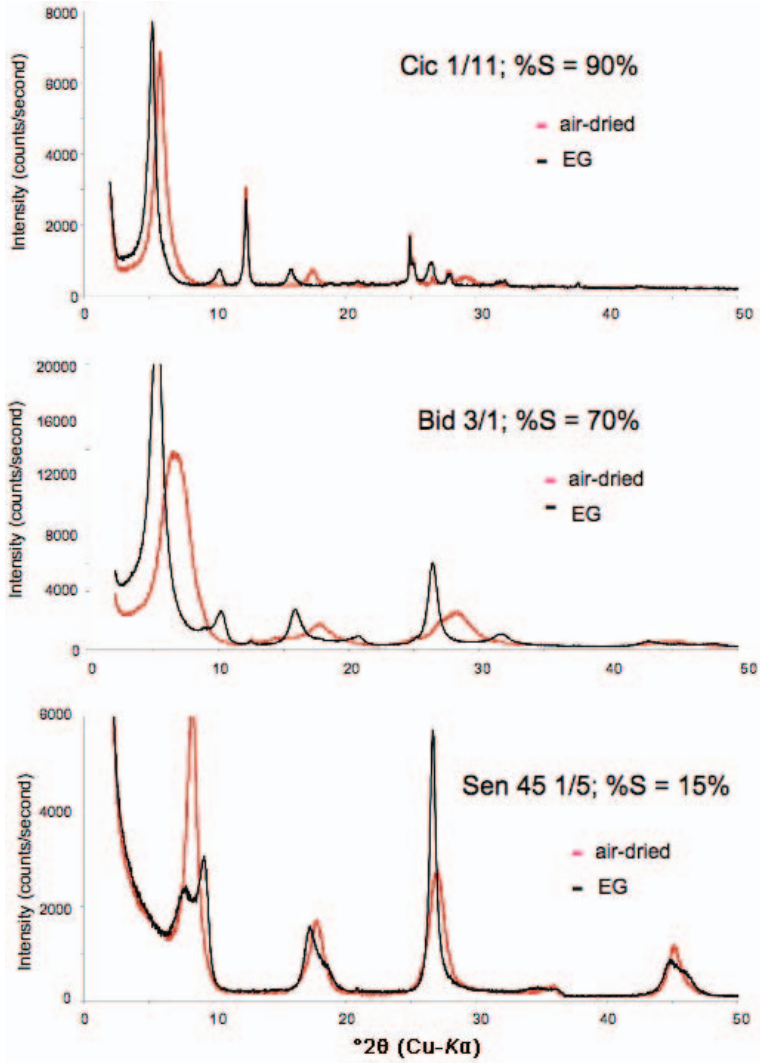

FIG. 4. XRD patterns of the <2 μm size fractions of samples Cic1/11, Bid1 3/1 and Sen45 with different expandability (%S) shown in the graphs. The two diagrams of each pattern correspond to the air-dried and ethylene-glycolated specimens.

https://doi.org/10.1180/claymin.2014.049.2.07 Published online by Cambridge University Press

to 30%S in sample Cic1/12. A significant amount of dioctahedral illite mixed with the I-S was also identified in sample Cic1/18 that does not conform to the expected smectite-to-illite trend. Interestingly, the highest illitization grade was found in the <2 μm fraction of sample Les2 collected at the shallowest depth of 1050 m. The abnormal grade of this sample was confirmed by the Ir index used to trace minute amounts of expandable layers in the I-S (Środoń & Eberl, 1984) that did not detect any smectite-type layers in the size fraction consisting exclusively of pure illite and kaolinite.

The %S of five <2 μm size fractions (Cic1/11, Cic1/18, Cic1/20, Trh1 and Ban13) plot along a straight line relative to present-day depth, confirming an illitization process driven by burial. Illitization seems to have occurred between ~1500 m (= 100%S in I-S) and ~3400 m (= 0%S in I-S). Seven other fractions (Cic1/12, Cic1/15, Ptr13, Ptr47, Sen13, Sen21 and Sen45) plot around a second sub-parallel line that also supports burial-driven illitization between ~500 m and ~2500 m depth (Fig. 5). Sample Bid1 plots between the two arrays and sample Les2 far above. Burial is confirmed to be the dominant controlling factor, but the results also suggest the influence of other parameters, as for the Cic samples collected next to the strato-volcano, and whose data points plot on the two lines, implying changing physical and and/or chemical conditions during crystal growth, and for the unexpected location of the illite fraction of sample Les2 with 0%S in I-S at a depth as shallow as 1000 m, implying an abnormally high thermal gradient during nucleation.

The %S was also determined for I-S of the <0.2 μm fraction of samples Cic1/11, Sen45 and Ptr47. The position and shape of the I-S peaks remained identical in all of these fractions (Fig. 4), indicating similar expandability in the two size fractions of the samples. The XRD patterns are identical, beside minor amounts of quartz detected in the coarser fraction. For sample Ptr47, some of the I-S peaks were less pronounced in the smaller fraction suggesting slightly higher expandability; minor amounts of quartz were detected in the <2 μm fraction. Expandability was not determined in the smaller fractions, as the infinite dispersion procedure applied to separate the nanometric illite-rich crystals theoretically broke the smectite-type bonds of the I-S.

The K-Ar ages

The K-Ar ages are variably scattered as expected for illite-rich crystals precipitated during burial-driven diagenesis, either decreasing or increasing with increasing particle size. They were split into two groups based on an arbitrary upper cut-off limit of 0.2 μm for the smaller nanometric particles. The larger micrometric aggregates were considered to consist of either nanometric particles with ages in the range of the individual nanometric particles, or naturally larger and older particles resulting from

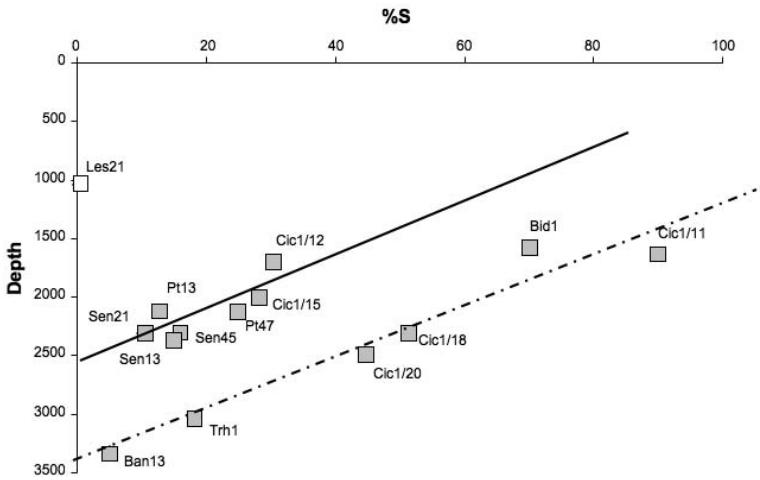

FIG. 5. Expandability of the illite-smectite mixed-layers (%S) *vs.* burial depth of the studied samples.

https://doi.org/10.1180/claymin.2014.049.2.07 Published online by Cambridge University Press

on-going illitization (Table 2). The K-Ar results of already published studies on the same I-S from similar bentonites of the same basin were also used to enlarge the database (Table 3). In the case of samples Cic1/15, Cic1/20, Les2, Trh1 and Sen45, the K-Ar age ranges of the coarser micrometric particles are within the age span of the nanometric particles, suggesting a possible occurrence of aggregates. For samples Cic1/11, Ptr47, Ptr13, Sen13 and Ban13, the micrometric size fractions yield older ages than the nanometric ones (Fig. 6). The following provisional remarks can therefore be made:

1. Illitization did not last equally long in most of the samples, even from the same well; for instance from 4.7 to 3.2 Ma in sample Cic1/15 and from 7.8 to 3.8 Ma in sample Cic1/20.

2. Illitization lasted for the same time in the nanometric fractions of the two Bid1 samples (from 10.6 to 6.3 Ma) and for the Sen13 and Sen21 samples (from 5.5 to 2.2 Ma); the micrometric fractions of the two Senné samples overlap the span of the nanometric and aggregates of sample Sen45 from 11.1 to 7.5 Ma.

3. Illitization of the nanometric particles lasted from as long as 4.9 Ma in sample Cic1/18 (or 4.3 Ma in sample Ptr47) to as short as <1 Ma in samples Cic1/11 and Ptr13 (or 1.3 Ma in sample Les2).

4. Illitization started either rapidly after deposition, within 2 Ma in samples Ban13 and Ptr47, or was significantly delayed, e.g. by more than 7 Ma in the sample Cic1/15.

The stable isotope results

Determination of $\delta^{18}O$ and δD for the different nanometric and micrometric particles provided also precise measurements (±10% of value) of the H_2O^+ content of the size fractions, and therefore of the amount of the hydrated layers probably of smectite type (Tables 2 and 3). The amounts increase slightly but consistently with grain size for samples Cic1/11, Les2 and Sen13, from 3.0 to 3.8, from 2.3 to 3.7 and from 3.2 to 3.6 μmoles/mg, respectively. By contrast, the H_2O^+ contents decrease from 3.3 to 2.1 μmoles/mg in sample Ptr13, and remain about constant between 3.5 and 3.7 μmoles/mg in sample Cic1/15. In fact, except for the 1–2 μm fraction of sample Ptr13, the overall H_2O^+ contents of the nanometric particles remain in a relatively narrow range from 2.8 to 3.8 μmoles/mg, implying that they are independent of the smectite content of the initial coarser I-S, and that the separation into illite-rich crystals succeeded (Table 1). In detail, the H_2O^+ contents of the

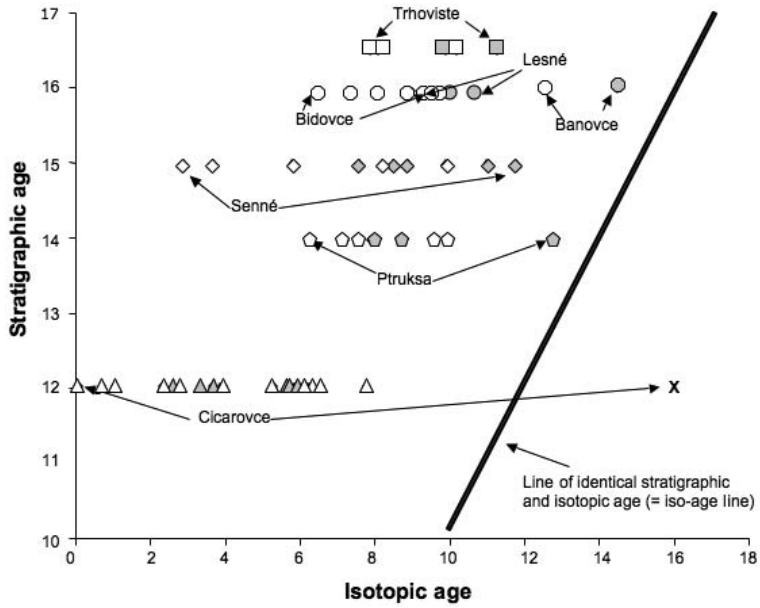

FIG. 6. K-Ar ages of the nanometric and micrometric size fractions of the studied bentonite beds relative to the stratigraphic age of the different samples. The grey symbols stand for the coarser size fractions and the cross for the sample with the suspected detrital contamination.

https://doi.org/10.1180/claymin.2014.049.2.07 Published online by Cambridge University Press

micrometric fractions of samples Cic1/11 and Ptr13, whose K-Ar ages suggest two illitization episodes, are different from those of the nanometric fractions.

The $\delta^{18}O$ values of the micrometric fractions of samples Cic1/11, Sen13 and Ptr13 are different from those of the nanometric fractions, confirming the previously suggested hypothesis of successive illitization episodes. The $\delta^{18}O$ values for the size fractions of sample Cic1/15, whose uniform K-Ar ages suggest that the micrometric fractions could correspond to aggregates of the nanometric crystals are distinctive, but they are within analytical uncertainty for the two nano- and micrometric categories. Conversely, the $\delta^{18}O$ ranges differ slightly but consistently for the micrometric and nanometric size fractions of other samples: from 11.7–11.8‰ to 12.2–12.6‰ (V-SMOW) in sample Cic1/15; from 13.4–14.3‰ to 14.6–15.1‰ in sample Cic1/11; from 15.7–16.6‰ to 14.8–15.5‰ in sample Ptr13; from 14.9–15.7‰ to 14.8–16.6‰ in sample Les2; and from 19.5–22.0‰ to 17.6–18.7‰ in sample Sen13.

The δD values do not change consistently with particle size. They range widely from −121‰ for the finest to −29‰ (V-SMOW) for the coarsest fraction of sample Les2. The data for the other samples are less scattered, decreasing when grain size increases for samples Cic1/15 and Cic1/11, or displaying no clear trend for samples Sen13 and Ptr13. Combining the $\delta^{18}O$ and δD isotopic data shows several relationships: (1) δD increases with grain size from −100 to −45‰ (V-SMOW) in sample Cic1/11 and from −77 to −38‰ in sample Cic1/15, whereas $\delta^{18}O$ remains almost constant; (2) δD increases with grain size from −121 to −29‰ in sample Les2, with a slight change in $\delta^{18}O$; (3) δD increases with grain size from −94 to −40‰ in sample Sen13, with an increase in $\delta^{18}O$ from 17.6 to 19.5‰; and (4) δD decreases when particle size increases from −42 to −86‰ in sample Ptr13, without a significant change in $\delta^{18}O$.

The combined K-Ar, $\delta^{18}O$ and δD data

When plotted against the K-Ar ages, the $\delta^{18}O$ values of the varied size fractions cluster around two sub-parallel lines with positive slope (Fig. 7a). The data for three samples are part of the lower array, while the nano-sized fractions of sample Cic1/11 and all data of sample Sen13 plot around the upper line. Interestingly, some micrometric size fractions of sample Cic1/11 plot close to data points of other samples.

When plotted against the K-Ar ages, the δD values form four groups at four different periods of approximately 11 Ma, 8 Ma, 4 Ma and 1 Ma (Fig. 7b). Again, some coarser micrometric fractions plot away from arrays drawn through the nanometric size fractions of the same samples. This is the case for the same Cic1/11 and Sen13 micrometric fractions noted in the previous paragraph, and for one Ptr13 coarse fraction. The data also show that the coarser fractions often have higher δD values. When particle size increases, the δD values often increase significantly, while the $\delta^{18}O$ do not vary or do so only slightly.

DISCUSSION

Correlated with the present-day depth of the samples, the expandability (%S) of the studied size fractions suggests that illitization occurred between ~1500 m and ~3400 m and between ~500 m and ~2500 m, depth, depending on the sample locations in the basin. Burial is confirmed to be the dominant driving parameter, but the results suggest also that the impact of changing thermal gradients is mainly due to the proximal volcanic activity, e.g. the occurrence of a pure illite in sample Les2 buried only to 1000 m depth. Evaluation of the K-Ar ages confirms that illitization is not a continuous process proceeding at the same time over the entire sampled area: diagenetic crystallization was not strictly contemporaneous for all samples, with an initiation variably delayed relative to time of deposition. Illitization obviously followed different pathways on the basis of decreasing or increasing K-Ar ages relative to particle size. The $\delta^{18}O$ results indicate that the nanoparticles from bentonite beds in different drill holes crystallized from fluids with changing characteristics. At least two types of fluids migrated through the bentonite beds and probably the surrounding sedimentary units. The $\delta^{18}O$ values from some micrometric size fractions also confirm that some of the studied I-S consists of two generations of nanoparticles and that crystallization temperature, fluid $\delta^{18}O$ and/or water/rock ratio varied during nucleation and growth.

These preliminary statements support the contention that if illitization is driven by burial with temperature increase and changing chemical composition of the migrating fluids, its commencement, duration and intensity were significantly variable from one place to another in the same

https://doi.org/10.1180/claymin.2014.049.2.07 Published online by Cambridge University Press

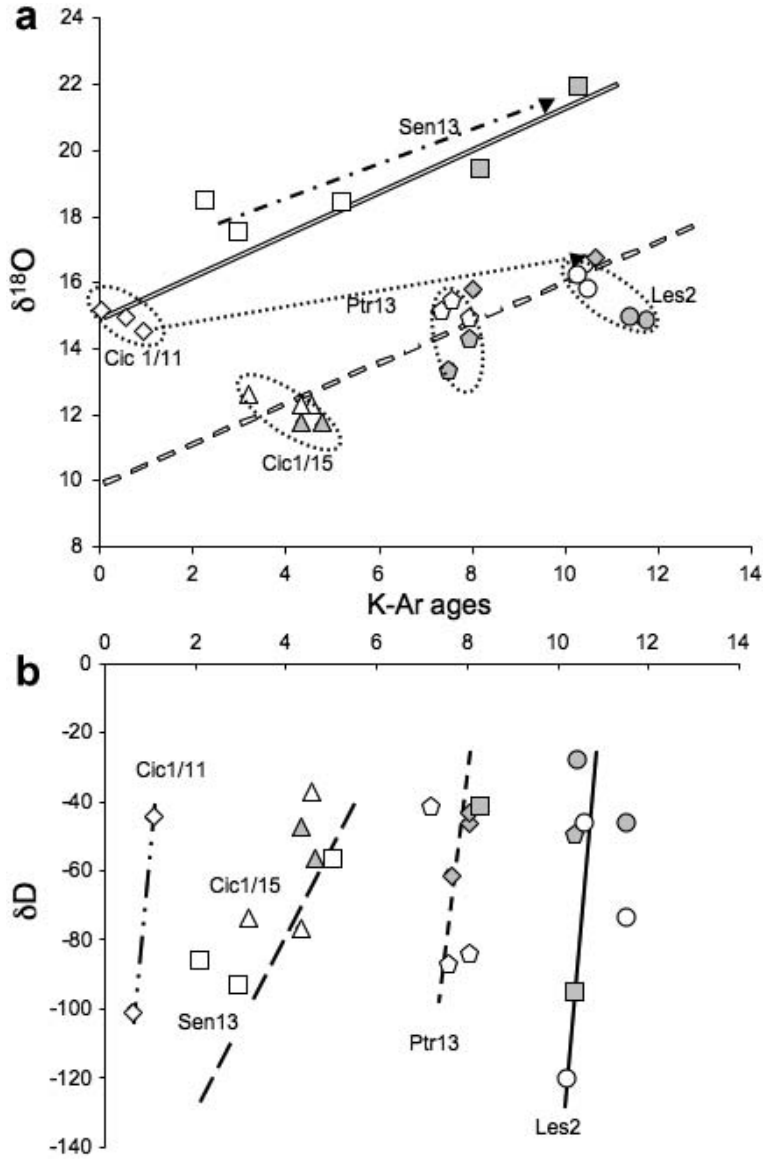

FIG. 7. (a) $\delta^{18}O$ and (b) δD data of the size fractions from samples Cic1/15, Cic1/11, Ptr13, Les2 and Sen13 relative to their K-Ar ages. The grouped values are surrounded by ovals, whereas the dispersed values are connected with arrows from smaller fractions towards the coarser in figure a. In both figures the grey symbols stand for the coarser fractions..

basin, and even within the same or closely spaced drill holes. The impact of the changing thermal gradient and subsidence rate on the degree of diagenesis, its duration, its continuity or discontinuity, as well as the changing fluids can be tentatively differentiated and evaluated. In this respect, the results and above statements provide the basis for two discussion topics, namely: (1) how protracted was illitization at a regional scale in the sedimentary basin? And (2) how can the regional evolution of the basin be evaluated on the basis of illitization at a regional scale? The K-Ar ages of nano- to micrometric illite-type particles from previous studies suggested that the micrometric

https://doi.org/10.1180/claymin.2014.049.2.07 Published online by Cambridge University Press

fractions (>0.2 μm) are most often on the older side of the K-Ar age range. With the larger data basis, most K-Ar ages of the micrometric size fractions are in the same age range as those of the nanometric size fractions for samples Cic1/15, Cic1/18, Cic1/20, Trh1, Ban13, Ptr13, Bid1 3/3 and Les2, whilst those for samples Cic1/11, Ptr47, Ban13, Sen13 and Sen21 are significantly older (Tables 2 and 3; Fig. 6). For the former set of samples, crystal growth seems to have occurred together with simultaneous nucleation in the sense of Eberl *et al.* (1998b). However, when the K-Ar ages of the micrometric particles are beyond those of the smallest particles, illitization could have occurred repetitively, the earliest inducing precipitation of particles that become the largest, while the youngest are the smallest (Fig. 6). The results obtained confirm that illitization can proceed repetitively in the same unit, probably depending on changes in local chemical and physical parameters.

Regional extent of illitization relative to time

Timing of illitization in the bentonite beds. Except for sample Cic1/12 that contains a nanometric fraction at ~16.0 Ma, slightly older than the stratigraphic reference, all nanometric fractions yield K-Ar ages that are younger than ~14 Ma. The 16 Ma age outlier has already been discussed for its probable contamination by detrital sedimentary material, e.g. possibly the dioctahedral illite (and chlorite) identified by XRD. The other K-Ar ages indicate that illitization lasted in the selected region of the East Slovak Basin from 14.5±0.9 to 0 Ma, in other words from soon after deposition until the present. A closer examination of the K-Ar ages shows specific local crystallization conditions and not a continuous process everywhere. For instance, illitization started soon after deposition in sample Ban13 at 14.5±0.9 Ma ~1.5 Ma after deposition and in sample Ptr47 at 12.3±0.1 Ma ~1.7 Ma after deposition, which corresponds roughly in both cases to the Middle Miocene subsidence. Except for sample Ban13, for which nanometric crystals precipitated at the same time as the micrometric particles, illitization started later at about 11.0±0.5 Ma in most of the other bentonite beds, and lasted for 8.2 Ma in samples Bid1 3/3 and Sen13, for 7.2 Ma in samples Thr1, Sen2 and Ptr13, and for 6.1 Ma in samples Bid1 3/1 and Ptr47. Interestingly, illitization started progressively in the Cic bentonites: at 9.5 Ma in sample Cic1/12, at 7.9±0.1 Ma in samples Cic1/20, Cic1/18 and Cic1/11, and at about 4.7 Ma in sample Cic1/15, not necessarily corresponding to a progressive burial, which implies the occurrence of other influencing parameters in addition to burial-induced temperature increase, volcanic pulses being a possibility. An ultimate, very recent record was detected in sample Cic1/11 between 0.6 and 0 Ma that can reasonably only be related to volcanic activity. The volcanic pulses produced ash plumes and heat flow. In summary, the K-Ar ages confirm that illitization was not a simple, single and continuous process. They also show that it started at different times after deposition and lasted variably in the different beds.

Burial-induced temperature being not the only driving parameter, illitization was active twice, from 8.0 to 7.6 Ma and from 0.6 to 0 Ma in sample Cic1/11, from 9.5 to 6.4 Ma in sample Cic1/12, from 4.7 to 3.2 Ma in sample Cic1/15, from 7.5 to 2.6 Ma in sample Cic1/18, and from 7.8 to 3.7 Ma in sample Cic1/20 (Tables 2 and 3). The process started about 10 to 8 Ma ago with a duration dependent on the thermal pulses and probably on the migration direction(s) of the related fluids. The idea that illite nanocrystals precipitating from associated interstitial fluids during successive illitization episodes yield ages younger than those of the coarser micrometric particles (Clauer, 2006) is supported here by the K-Ar results of the Cic1/11, Sen13 and Sen21 fractions, where two diagenetic episodes were identified. Honty *et al.* (2004) postulated independently a continuous growth of the illite-rich nanoparticles with asymptotic size distribution patterns for most of the samples, by using the GALOPER computer program (Eberl *et al.*, 2001) and plotting the α and β^2 parameters of the size fractions (mean and variance of the natural logarithms of the thicknesses) in a diagram, along with other previously obtained results, to evaluate the crystal growth reaction paths according to the theory of Eberl *et al.* (1998b) (Fig. 8). The data points of the clay particles of most samples plot along the line defining a combined nucleation and growth process, whereas the clay fractions of only two samples, namely Trh1 and Sen21, appear to have resulted from a surface-controlled growth process. This discrepancy in the crystallization process needs to be addressed in future, probably by a more dedicated analysis of the correlation

https://doi.org/10.1180/claymin.2014.049.2.07 Published online by Cambridge University Press

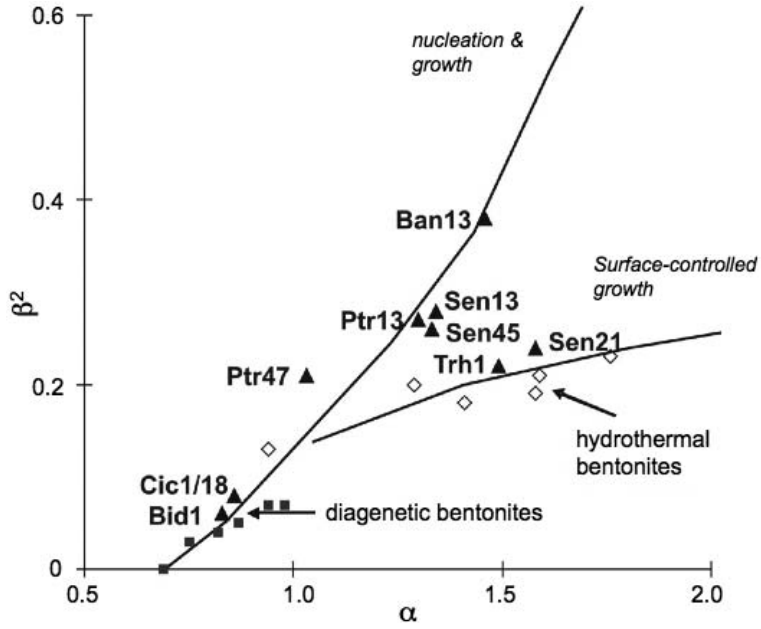

FIG. 8. α *vs.* β^2 plot of the <2 μm size fractions of different samples using the BWA-PVP and HRTEM-PVP techniques. See text for explanation. The two sets of data points for diagenetic and hydrothermal bentonites are from Środoń *et al.* (2000) and Eberl *et al.* (1998b), respectively. The size fractions studied here are labelled in the diagram.

between asymmetry and ages of the particle-size distribution. As for the K-Ar results, crystal aggregates of different K-Ar ages might slightly bias the distribution patterns.

Chemistry of the fluids during illite nucleation and growth. The oxygen and hydrogen isotopic compositions of the authigenic crystals are dependent on the chemistry of the interacting fluids and on the crystallization temperature. Interaction with organic matter is not considered a significant process here. In confined systems, as is the case for these bentonitic materials, the mineral $\delta^{18}O$ should decrease during crystal growth when either the temperature or the water/rock ratio increases (Eslinger & Savin, 1973; Savin & Lee, 1988; Whitney & Northrop, 1988; Bechtel & Hoernes, 1990; Girard & Barnes, 1995; Delgado & Reyes, 1996; Sheppard & Gilg, 1996). In the described nucleation/growth process, most measured $\delta^{18}O$ and δD values tend to increase with particle size (Table 2), confirming an increase of the temperature or the water-rock interaction, or both, unless the isotopic composition of the interacting pore fluids changed. In low-permeability bentonite units, the isotopic composition of the parental fluids could have varied locally and temporally, adding to the complexity of the distribution of the clay-mineral data. Diffusion and isotope exchange during water-rock interactions may also have contributed to fluid isotope variability, the former being less likely than the latter.

As bentonite beds are characterized by relatively low porosity (<18%) and extremely low cation diffusion rates (10^{-11} to 10^{-13} m^2/sec), local chemical fluid heterogeneities could have influenced the $\delta^{18}O$ and δD values of initial crystals of probable smectite-type that nucleated and grew as a result of initial alteration of the volcanic glass. This reasoning is based on the $\delta^{18}O$ increase with particle size in samples Sen13 and Ptr13 that had no evidence for subjection to a significant temperature decrease relative to the other samples. Alternatively, any change in the water/rock ratio would suggest an open system behaviour, which seems not to have been the case here given the rock type. However, as illitization was sometimes episodic, changes in $\delta^{18}O$ and δD are expected, especially in sample Cic1/11 where very recent illitization could have been linked to interaction with meteoric waters. Therefore, illitization in the

https://doi.org/10.1180/claymin.2014.049.2.07 Published online by Cambridge University Press

bentonite beds and in the surrounding shales could favour oxygen and hydrogen isotope exchange between the interstitial fluids from surrounding shales and the initial smectite of the bentonite units.

Further elucidation of these issues is shown in Fig. 7 where the data plots suggest that timing and duration of illite growth could also influence the mineral $\delta^{18}O$. For those locations with a short duration of illitization such as for samples Les2 and Cic1/15, the $\delta^{18}O$ value is low and the scatter narrow, at 15.7±0.7 ‰ and 12.1±0.3‰ (V-SMOW at ±1σ), respectively. On the basis of the burial history of sample Sen13 (as in Fig. 3), from which the temperature interval extends from 110 to 130ºC over the 11 to 2 million years time span, the change of the mineral $\delta^{18}O$ can be tentatively quantified. Inserting the temperatures into the illite-water equilibrium oxygen isotope fractionation equation (Sheppard & Gilg, 1996):

$$1000\ln\alpha^{18}_{\text{illite-water}} = 2.39 \times 10^6 T^{-2} - 3.76$$

gives respective fractionations of 12.1‰ and 10.5‰ that differ by only 1.6‰ compared to the observed mineral $\delta^{18}O$ range of 4.4‰. If illite precipitated at isotopic equilibrium, the $\delta^{18}O$ of the parental fluid had therefore to change significantly during crystal growth. One can elaborate on this argument by assuming that burial rate was approximately linear relative to time, allowing interpolation of temperatures for each measured illite age, and calculation of $\delta^{18}O_{water}$ for each measured clay mineral $\delta^{18}O$ (Table 4). The mean water $\delta^{18}O$ of around 8‰ points to an isotopically evolved parental fluid, presumably becoming enriched in ^{18}O during water-rock interaction in a rock-dominated system (e.g. Aagard & Egeberg, 1998). Here, this interaction consisted probably of cation exchange by smectite, resulting from the alteration of the initial volcanic glass. Based on a mean temperature of 120ºC, a calculation of the water $\delta^{18}O$ of the other samples gives 0.9‰ for the sample Cic1/15; 2.7‰ for the micrometric fractions of the sample Cic1/11; 3.7‰ for the nanometric fractions of the same sample Cic1/11; 4.5‰ for the sample Les2, and from 3.9 to 5.4‰ for the sample Ptr13. In turn, the lowest calculated value of 0.9‰ for sample Cic1/15 suggests a contribution from surface-derived waters (e.g. Sheppard, 1986).

Coupling this conclusion to the duration of illitization that can be short (e.g. at 10.9±0.6 Ma for sample Les2 and 4.2±0.5 Ma for sample Cic1/15, each with 1σ uncertainty), or long (e.g. spanning from 2.2 to 10.3 Ma in sample Sen13), explains why there are consistent relationships in the $\delta^{18}O$ *vs.* K-Ar age plot (Fig. 7a). Two data arrays can be distinguished: a group comprising all size fractions of the sample Sen13 and the three finest size fractions of the sample Cic1/11, and another group with the rest of the results. Regressing the $\delta^{18}O$ and K-Ar age data (τ) gives:

$$\delta^{18}O = 15.2 + 0.6\tau$$

for the first group of data with $r = 0.9164$, which is significant above the 95% level for $n = 8$, and

$$\delta^{18}O = 10.2 + 0.5\tau$$

for the second group of data with $r = 0.8470$, which is significant above the 99.9% level for $n = 16$. The fact that the best-fit lines are in essence parallel might be indicative of secular changes in two pore-fluid $\delta^{18}O$ regimes at rather constant rates. Such an interpretation is admittedly speculative given that some of the variation is also due to temperature influence and that the co-variation arises from grouped $\delta^{18}O$ aggregates during the short episodes of illitization.

TABLE 4. Calculation of $\delta^{18}O$ of the fluids for each measured clay mineral $\delta^{18}O$ relative to timing and estimated crystallization of the illite-type particles.

Time (Ma)	Temperature (ºC)	$10^3\ \ln\alpha^{18}O_{\text{illite-water}}$	$\delta^{18}O_{\text{illite}}$	$\delta^{18}O_{\text{water}}$
2.2	130	10.5	18.7	8.2
3.0	128	10.7	17.6	6.9
5.1	123	11.1	18.4	7.3
8.2	115	11.7	19.5	7.8
10.3	110	12.1	22.0	9.9

https://doi.org/10.1180/claymin.2014.049.2.07 Published online by Cambridge University Press

The δD data presented herein are among the first published for nanometric illite-rich crystals to the best of our knowledge. There is still a debate about the significance and extent of hydrogen isotopic fractionation in clay-type particles (e.g. Savin & Lee, 1988) so that the following discussion is speculative to some extent. As the nanometric particles nucleated and grew probably in connection with limited amounts of pore fluids, the same rules as for oxygen isotope partitioning should apply. Negative correlations between $\delta^{18}O$ and δD should also appear with increased temperature during crystal growth, possibly influenced by the occurrence of minute amounts of contaminant minerals, and other processes, e.g. salt effects (Fig. 5). The hydrogen isotope data plotted against K-Ar ages (Fig. 7b) and against the H_2O^+ contents (Tables 2 and 3) show no discernible trends with an overall scatter from –20 to –120‰. The relatively tight grouping in $\delta^{18}O$ data for short-lasting illitization is not replicated in the δD values. Water–rock interactions, including chemical reactions like hydration, are generally responsible for variations in pore fluid $\delta^{18}O$ and can have an even greater effect on D/H in low porosity, low permeability rock environments. The trends are very restricted when illitization was short lasting, such as in samples Cic1/15, Ptr13 and Les2, and wider when illitization lasted longer such as for the sample Sen13, or was episodic such as for the sample Cic1/11, suggesting again isotopic changes during illitization of variable duration. As the δD data show a mode at about −45‰ with half of the measurements within the range –45±15‰ (Fig. 9), the clay mineral-water hydrogen isotope fractionation factor suggested by Capuano (1992) may be used with a mean temperature of 120ºC:

$$1000\ln\alpha^{D}_{\text{clay-water}} = -45.3 \times 10^{3}/T + 94.7$$

to give a fractionation of −21‰ and a water δD of around −24‰ for a measured mineral δD of −45‰. Such a value is consistent with a surface-derived fluid (plausibly seawater) as proposed earlier on the basis of the oxygen isotope data. Most of the other δD data outside of the −45±15‰ range skew to low δD values independent of locality and grain size (Fig. 9). O'Neil (1992) highlighted the "extraordinarily high" rates of hydrogen isotope exchange between hydrous minerals and molecular hydrogen in laboratory experiments. Given the expected low D/H of naturally produced but highly reactive hydrogen here, perhaps there might be a role for that evanescent species in producing low δD clay minerals.

Similar to the K-Ar ages, the $\delta^{18}O$–δD results do not support the overwhelming occurrence of agglomerated nanometric particles in the micrometric size fractions, as the data are widely scattered. The data plot shows $\delta^{18}O$ changing marginally when the size fractions change, while δD changes significantly. The results from coarser micrometric

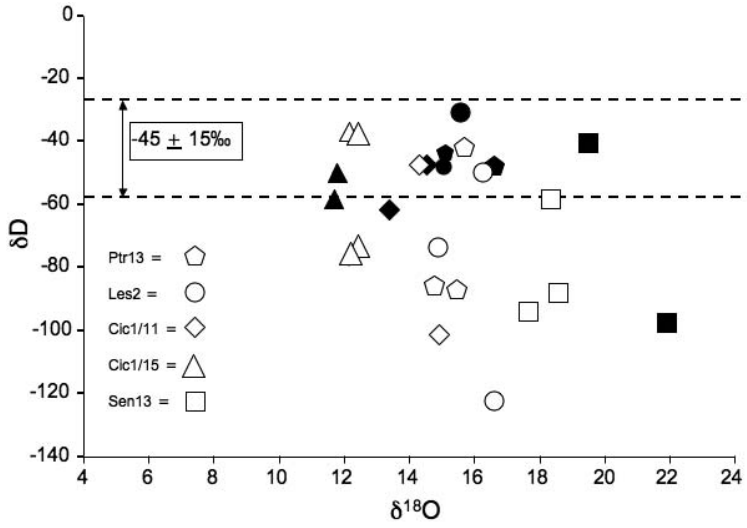

FIG. 9. $\delta^{18}O$ *vs.* δD data of the studied size fractions framed by a range of −45±15‰ containing most of the analysed size fractions. The full symbols stand for the coarser size fractions.

https://doi.org/10.1180/claymin.2014.049.2.07 Published online by Cambridge University Press

fractions mostly plot in the above-defined −45±15‰ area (the full symbols of Fig. 9). If temperature changes are mainly recorded by $\delta^{18}O$ of the particles, and if other effects, not yet necessarily all identified, are mainly recorded by δD, the data indicate that the temperature did not change dramatically during crystal growth in most of the studied samples, but other factors could have varied, depending for instance on the immediate environment of the nucleating and growing crystals. The temperature change during particle growth remains to be evaluated for each sample. Several independent approaches can be applied for estimation of the crystallization temperature. The approach elaborated by Šucha *et al.* (1993), which is based on the amount of expandable layers in the I-S structures relative to depth and derivation of a palaeotemperature from depth, suggests that the temperature ranged between 70ºC for sample Cic1/11, and 115ºC, at the most, for sample Les2 that no longer contains expandable layers and should have been subjected to a temperature of at least 200ºC (Tables 3 and 4). On the basis of oxygen isotope fractionation calculations between illite and water by Eslinger & Savin (1973) and Lee (1984) that take into account a bond-type approach combined with data on natural samples, the maximum temperatures reached during illitization could have varied from as low as about 50ºC for sample Sen13, which might be too low, to as high as about 140ºC for sample Cic1/15 (Tables 2 and 3). The third approach based on the subsidence backstripping from some wells and the vitrinite reflectance data provides temperatures ranging from as low as about 70ºC in sample Les2, which is again too low for an I-S structure without expandable layers, to 135ºC in sample Trh1 (Table 5). This provides support for Essene & Peacor (1995) who advocated that the amount of smectite layers in the I-S structure should not be used as a palaeotemperature indicator. The calculated temperatures are reasonably similar for the stable isotopic and backstripping approaches but not for estimates based on expandability. Therefore, temperature is obviously not the only determining parameter for the burial-induced degree of illitization.

The differences could, of course, result from variations in the initial $\delta^{18}O$ compositions of the interstitial fluid. To reduce and even erase such differences, the $\delta^{18}O$ of the fluids should then vary during the illitization process at the different sampling sites, which can at least partially result from changing water/rock interactions, from thermal gradient, or from other processes not yet identified. Beyond these aspects that cannot yet be fully addressed, it can be suggested that differences in the nucleation and growth processes may induce changes in δD, and therefore could result in changing $\delta^{18}O-\delta D$ compositions of the hydroxyls because of interactions between fluids and minerals as the size of the particles increases. Whilst the capacity for isotope resetting during post-precipitation processes is still debated, D/H is expected to be more susceptible to change than $^{18}O/^{16}O$ (e.g. Bird & Chivas, 1988; Longstaffe & Ayalon, 1990, and references therein).

Some of the measured $\delta^{18}O$ values, and even more of the δD, might therefore relate to changing OH radicals at least during crystal growth, but possibly also during nucleation, indicating significant changes in the available oxygen and hydrogen during long-lasting illitization. Bechtel & Hoernes (1990) estimated that isotope fractionation between framework and hydroxyl oxygen in illite is about 15‰ at 200ºC, and even higher at lower temperature. Changes in the fraction of oxygen contributed by the hydroxyls can thus affect the bulk $\delta^{18}O$, but smectite layers may also preserve interlayer water of an isotopic composition acquired from the environment prior to illitization. In some cases, this initial composition could be isotopically distinct from that of the fluid present during illitization and yet contribute to the final composition of illite. Part of the isotope changes could, therefore, also have been induced by a solid-state alteration of smectite layers into illite layers of I-S during crystal growth, rather than an addition of nucleating illite layers to the original smectite layers during particle growth.

Illitization records and evolution of the East Slovak Basin

Impact of salt-bearing fluids on crystallization of the I-S nanoparticles. Another topic for this discussion is the potential impact of saline fluids, such as those reported by Honty *et al.* (2004), on the K-Ar and stable isotope systematics of nucleating and growing illite crystals. Because of isotope partitioning between water molecules involved in the hydration process and those in the remaining bulk water, the stable isotope fractionation factors between minerals and fluids that were calculated above may need to be corrected for a "salt effect" due, for instance, to solute-solvent

https://doi.org/10.1180/claymin.2014.049.2.07 Published online by Cambridge University Press

TABLE 5. Information from backstripping combined with the timing of the onset of illitization, the calculated depth at the onset of illitization and the subsidence rates.

Sample identification	Sample IDs	Deposition age (in Ma)	Depth (in m)	Information from backstripping (burial depth at given time)	Onset of illitization (in Ma)	Depth at onset of illitization (in m)	Subsidence rate* (m/Ma)
Salt-free samples							
Cicarovce 1/11	Cic1/11	12.5–11.5	1614	1000 m at 11.5 Ma + 1250 m at 11 Ma + 1500 at 8.5 Ma	8.0 + 0.6	1550 + 1600	390 + 140
Cicarovce 1/12	Cic1/12	13.0–12.0	1703	800 m at 11 Ma + 1500 m at 8 Ma	9.5	1205	400
Cicarovce 1/15	Cic1/15	13.0–12.0	2002	the same by approximation	4.7	1820	230
Cicarovce 1/18	Cic1/18	13.5–12.5	2296	1000 m at 12.5 Ma +1600 m at 11 Ma + 2250 m at 5.5 Ma	7.5	1835	335
Cicarovce 1/20	Cic1/20	13.5–12.5	2495	1000 m at 12.5 Ma +1600 m at 11 Ma + 2250 m at 5.5 Ma	7.4	1835	330
Trhoviste 1/37	Trh1	17.0–15.5	3015	1000 m at 15 Ma + 3000 m at 11 Ma	11.3	2850	530
Salt-bearing samples							
Bidovce 1 3/1	Bid1 3/1	16.5–15.5	1557	1000 m at 14 Ma + 1500 m at 14.5 Ma by approximation	10.2	1515	260
Bidovce 1 3/3	Bid1 3/3	16.5–15.5	1565	the same by approximation	10.6	1515	280
Senné 21 4/1	Sen21	15.5–14.5	2311	410 m at 13.5 Ma + 1200 m at 12.5 Ma + 1625 m at 11 Ma + 2175 m at 5.5 Ma	11.1 + 5.5	1625 + 2175	420 + 230
Senné 45 1/5	Sen45	15.5–14.5	2350	the same by approximation	9.2	1900	320
Senné 13 5A 2–1	Sen13	15.5–14.5	2402	the same by approximation	10.3	1695	360
Lesné 2 1A/3	Le2	16.5–15.5	1048	1000 m at 15 Ma + 3000 m at 11 Ma	11.6	1000 ?	295
Banovce 13/12	Ban13	16.5–15.5	3313	the same by approimation	14.5 + 12.5	965 + 2250	645 + 640
Ptruksa 13 14	Ptr13	14.5–13.5	2100	1000 m at 12.5 Ma +1600 m at 11 Ma + 2250 m at 5.5 Ma	10.6	1670	490
Ptruksa 47 9/7	Ptr47	14.5–13.5	2106	the same by approximation	12.3 + 5.9	1240 + 2205	730 + 270

* based on the ratio between deposition depth and illitization onset

interactions (e.g. Graham & Sheppard, 1980; O'Neil & Truesdell, 1991). Such effects can be quantitatively significant (Horita *et al.*, 1993a,b) and under most circumstances, unless a brine correction is applied, fluid reconstruction ($\delta^{18}O$ and δD) from measured values of authigenic mineral phases will be underestimated by an amount depending on the solution composition. For the present purposes, it may be as well just to suggest possible "salt effects" as another source of variation in the measured isotopic compositions.

The degree of illitization relates to the salinity of the waters, as already discussed, with the enhanced illitization in the "salt-bearing" samples resulting from a higher crystallization temperature relative to the "salt-free" samples (Honty *et al.*, 2004). No additional heat source was involved for illitization in the salt-bearing beds because: (1) no volcanic activity was reported next to the "salt-bearing" samples; and (2) any external heat source would have also affected the degree of illitization in the shales hosting the salt-rich bentonite beds, whereas comparison with existing data for the shales of the East Slovak Basin shows no detectable difference in both burial and thermal gradients (Franců *et al.*, 1990; Šucha *et al.*, 1993). Although probably related to some local and limited temperature increase, salinity may be excluded as the factor leading to illitization immediately after deposition, as reported for salty and/or alkaline lakes (Singer & Stoffers, 1980; Deconinck *et al.*, 1988; Hay *et al.*, 1991; Turner & Fishman, 1991). The time-temperature pattern of the salt-bearing bed of sample Sen45 (Fig. 2) shows a similar temperature increase to that of the salt-free bentonite beds (Clauer *et al.*, 1997). The shallowly buried salt-rich bentonite beds containing the two Bid1 samples have an I-S expandability fitting the general trend of the "salt-free" samples, which also suggests that the impact of a salt-rich environment on the mineral expandability may become apparent after reaching a certain, but so far unknown, threshold temperature (Honty *et al.*, 2004). The K-Ar ages of the illite nanometric particles from both salt-bearing and salt-free samples overlap, suggesting that salty brines did not affect their K-Ar system. Also, Środoń (1984) did not report any effect of the saline/hypersaline environment on illitization in the shallow Miocene Carpathian fore deep.

Relatively high fluid $\delta^{18}O$ estimates obtained for the size fractions of samples Sen13, Les2 and Ptr13 are associated with salt-bearing situations, whereas salt-free situations are associated with lower fluid $\delta^{18}O$ estimates of the size fractions from samples Cic1/11 and Cic1/15. This may be, at least in part, an inherited distinction caused by water evaporation leading to an increase in $\delta^{18}O$ during brine formation prior to modification and later overprinting water-rock interactions.

Illitization and burial history. By comparing the stratigraphic age of the different bentonite beds with the illite K-Ar ages, illitization appears to be often related to subsidence episode(s) at basin scale (Table 4). This is recorded in samples Trh1, Sen21, Les2 and Ptr47, with an onset coinciding with the Middle Miocene (Lower Sarmatian) subsidence. In samples Bid1 and Ptr13, the illite K-Ar ages indicate that illitization was delayed relative to these subsidence episode(s). Only the Cic samples provide K-Ar ages for illitization that are significantly after the Lower Sarmatian subsidence. Therefore, the process could also relate to episodic thermal pulses induced by nearby volcanic activities. In the case of sample Ban13, the first illitization relates to the Middle Miocene (Middle Badenian) subsidence, whereas the subsequent episode relates to the Lower Samartian subsidence.

An approximate depth at which illitization started can therefore be evaluated based on the back-stripping information and the illite K-Ar ages (Table 5). The overburden varies from 965–1000 m for samples Ban13 and Les2 to 2850 m for sample Trh1 (due to a thermal gradient of about 47ºC/km combined with a subsidence rate of about 275 m/Ma). Combining the timing of illitization in the bentonite units of the different wells, the depth where it occurred and the subsidence rate based on the ratio between depth and the initial K-Ar age gives an insight into how the basin evolved (Tables 5 and 6). Calculation of the subsidence rates gives three sets of values: (1) a high rate (>500 m/Ma) for samples Trh1 and Ban13, and before initial illitization in sample Ptr47; (2) an intermediate rate (from 500 to 300 m/Ma) for samples Cic1/12, Cic1/18 Cic1/20, Sen45, Sen13, Ptr13 and before initial illitization in samples Cic1/11 and Sen21; and (3) a low rate (<300 m/Ma) for samples Cic1/15, Bid1 3/1, Bid1 3/3 and Les2 and before second illitization in samples Cic1/11, Sen21 and Ptr47. These results are consistent, with subsidence rates quite close to samples from the same drill hole: i.e. for the Bid1, Sen13 and Sen45 samples, and most of the Cic samples with values between 330 and 400 m/Ma.

https://doi.org/10.1180/claymin.2014.049.2.07 Published online by Cambridge University Press

TABLE 6. Information from vitrinite reflectance and comparison of the expected temperature with those calculated from %S and evaluated at the onset of the illitization, as well as the consequent thermal gradients.

Sample identification	Sample IDs	Deposition age (in Ma)	Depth (in m)	S_{XRD} (%) + TºC *	Information from vitrinite reflectance (burial depth at given time)	Temperature at onset of illitization (ºC)	Thermal gradient (ºC/km)
Salt-free samples							
Cicarovce 1/11	Cic1/11	12.5–11.5	1614	90–70	65ºC at 1000 m + 70ºC at 1250 m + 80ºC at 1500 m	80 +85	45 + 47
Cicarovce 1/12	Cic1/12	13.0–12.0	1703	30–75	60ºC at 800 m + 95ºC at 1500 m	85	62
Cicarovce 1/15	Cic1/13	13.0–12.0	2002	28–95	the same by approximation	105	52
Cicarovce 1/18	Cic1/18	13.5–12.5	2296	51–90	65ºC at 1000 m + 90ºC at 1600 m + 120ºC at 2250 m	100	48
Cicarovce 1/20	Cic1/20	13.5–12.5	2495	45–90	65ºC at 1000 m + 90ºC at 1600 m + 120ºC at 2250 m	100	48
Trhoviste 1/37	Trh1	17.0–15.5	3015	18–100	70ºC at 1000 m +140ºC at 3000 m	135	44
Salt-bearing samples							
Bidovce 1 3/1	Bid1 3/1	16.5–15.5	1557	70–80	60ºC at 1000 m + 80ºC at 1500 m by approximation	80	46
Bidovce 1 3/3	Bid1 3/3	16.5–15.5	1565	70–80	the same by approximation	80	46
Senné 21 4/1	Sen21	15.5–14.5	2311	10–105	35ºC at 400m + 80ºC at 1200 m + 105ºC at 1625 m + 125ºC at 2175 m	105 + 125	58 + 52
Senné 45 1/5	Sen45	15.5–14.5	2350	15–105	the same by approximation	115	55
Senné 13 5A 2–1	Sen13	15.5–14.5	2402	15–105	the same by approximation	105	56
Lesné 2 1A/3	Le2	16.5–15.5	1048	0–115	70ºC at 1000 m +140ºC at 3000 m by approximation	70 ?	60
Banovce 13/12	Ban13	16.5–15.5	3313	5–110	70ºC at 1000 m +140ºC at 3000 m by approximation	65 + 115	57 + 47
Ptruksa 13 14	Ptr13	14.5–13.5	2100	13–105	80ºC at 1500 m + 110ºC at 2000 m	90	48
Ptruksa 47 9/7	Ptr47	14.5–13.5	2106	25–100	the same by approximation	95 +115	48 + 48

* TºC = average nucleation temperature based on % of S_{XRD} and 70ºC for start of illitization (Šucha *et al.*, 1993).

The thermal gradients can be grouped in the same way: high (>60ºC/km) for samples Cic1/12 and Les2; intermediate (from 60 to 50ºC) for samples Cic1/15, Sen21, Sen45, Sen13 and before initial illitization for sample Ban13; and low (<50ºC) for samples Cic1/11, Cic1/18, Cic1/20, Trh1, Bid1 3/1, Bid1 3/3 and Ban13, and before the second illitization for samples Ptr13 and Ptr47. There is again a consistency among the rates of three Sen samples, two Bid samples, two Ptr samples; three Cic samples also have narrowly constrained values. It emerges from comparing subsidence rate and thermal gradient, that the high values of one parameter are linked with the low values of the other one (such as in samples Trh1, Ban13, Ptr47, Les2), the intermediate values for both parameters being for the three Sen samples.

Distinct illite and fluid $\delta^{18}O$ values were observed at the same time at different locations, for instance at around 8 Ma for samples Sen13, Ptr13 and Cic1/11 (Fig. 7a), demonstrating a strong compartmentalization of the basinal fluids. This applies also for the Cicarovce-1 well where samples Cic1/11 and Cic1/15 have distinctly different illitization histories: there are local controls on the timing and duration of illitization. This heterogeneous situation for nearby confined bentonite units contrasts with basin-wide sedimentary sequences in which fluid connectivity is on a larger, continuously porous scale (e.g. in sandstone aquifers and hydrocarbon reservoirs): the stable isotope compositions of nanometric-sized illite particles from bentonites give a different insight into the fluid-temperature regime in elucidating local processes rather than delineating large-scale regimes. Episodic illitization in variously buried bentonite beds highlights again an older concept of "punctuated" diagenesis suggested by Morton (1985) for shales from the Gulf Coast. Here, the key concept is the effective fluid-rock ratio in the rocks during authigenic nucleation and growth, coupled with the specific fluid isotope composition and the ambient temperature, all parameters not systematically impacting illitization together. However, high effective fluid-rock ratios (e.g. in aquifers and oil-bearing reservoirs), when the oxygen isotopic composition of the authigenic mineral phases is buffered by the fluid, or low effective fluid-rock ratios when buffering is more likely by the rock, cannot be approached or differentiated during the evolution of a basin compartment, especially as time and reaction progress, on the sole basis of the stable isotope composition of the authigenic minerals.

CONCLUSIONS

K-Ar isotope dating and oxygen/hydrogen isotope characterization of nanometric and micrometric illite crystals of bentonite beds from the East Slovak Basin confirm that illitization is a complex crystallographic and chemical process. Progressive burial temperature increase together with chemical changes in the composition of the interstitial brines are the driving parameters controlling the process, but the combined effect of changing kinetic parameters, thermal gradients and water/rock ratios make the interactions very challenging to decipher.

In the East Slovak Basin, the onset of illitization relates to the Middle Miocene (Serravallian = Lower Sarmatian) subsidence between 13.5 and 11.5 Ma in most of the sampled bentonite beds, but it can also start either before or after this subsidence episode. On the basis of subsidence rates ranging from less than 300m/Ma to more than 500 m/Ma, and depending on the depth to which the bentonite beds were buried when illitization started, the thermal gradients range from as high as 60ºC/km to less than 50ºC/km. Low subsidence rates correlate with high thermal gradients and vice versa. Also, short-lasting illitization proceeded shortly after sedimentation, whereas long- to very long-lasting illitization occurred long after sedimentation, although this is a general observation rather than a strict rule. The amount of smectite layers in the illite-type mixed-layer structure gives erroneous estimations of the palaeotemperatures in bentonites affected by a salt environment, while the values of the vitrinite reflectance and the oxygen fractionation between illite and water, both provide values ranging from about 70 to 135ºC.

The $\delta^{18}O$ changes little as crystal size changes, whereas δD changes significantly. Temperature did not change significantly during crystal growth in most of the samples, but other effects such as the oxygen and hydrogen isotopic composition of the interacting fluids impacted variably on the $\delta^{18}O$ and δD of the authigenic illite crystals depending on the immediate environment of the samples, and the timing and duration of illitization.

The enhancing effect of a salty environment on the smectite to illite transformation trend was also documented in salt-bearing compared to salt-poor

https://doi.org/10.1180/claymin.2014.049.2.07 Published online by Cambridge University Press

volcanoclastics. The illite-type fundamental nanoparticles show a stronger illitization in the salt-bearing units, but the duration of the process does not appear to have been affected significantly. However, the oxygen and hydrogen isotope characteristics of saline fluids modified the stable isotopic characteristics of the nanometric and micrometric illite-rich particles.

Local controls on the timing and duration of illitization in relatively low-permeability bentonite beds of the East Slovak Basin contrast with large-scale fluid connectivity such as in sandstone aquifers and hydrocarbon reservoirs. The variable stable isotope compositions of nucleating and growing nanometric illite-type particles of bentonite beds gives a new insight into the fluid-temperature regime by identifying local processes rather than large-scale processes. The key concept considered here is the effective fluid-rock ratio in the rocks during nucleation and growth of authigenic clay-type crystals.

ACKNOWLEDGMENTS

We are very indebted to Ray Ferrell Jr., Louisiana State University, for his thorough review, as well as Harry Shaw, Imperial College, for his help during the review round and for editing some of the oral presentations of the 2011 Cambridge Conference on Diagenesis. We would also like to thank Raymond Wendling of the Centre de Géochimie de la Surface (CNRS/ULP) for technical assistance with the K-Ar measurements, as well as Chris Taylor of SUERC for technical assistance with the stable isotope measurements.

REFERENCES

Aagard P. & Egeberg P.K. (1998) Formation waters and diagenetic modifications: General trends exhibited by oil fields from the Norwegian shelf – A model for formation waters in oil prone subsidising basins. Pp. 281–284 in: *Water-Rock Interaction WRI-9* (G.B. Arehard & J.R. Hulsten, editors), Balkema, Rotterdam.

Altaner S.P. & Ylagan R.F. (1997) Comparison of structural models of mixed-layer illite/smectite and reaction mechanisms of smectite illitization. *Clays and Clay Minerals*, **45**, 517–533.

Aronson J.L. & Hower J. (1976) Mechanism of burial metamorphism of argillaceous sediments: 2. Radiogenic argon evidence. *Geological Society of America Bulletin*, **87**, 738–744.

Baráth I., Kováč M., Soták J. & Lankreijer A. (1997) Tertiary collision, metamorphism and basin forming processes in the Eastern Slovakia (central Western Carpathians). Pp. 65–78 in: *Geological Evolution of the Western Carpathians* (P. Grecula, D. Hovorka & M. Putiš, editors). *Mineralia Slovaca, Monograph*, Bratislava.

Bechtel A. & Hoernes S. (1990) Oxygen isotope fractionation between oxygen of different sites in illite minerals: A potential single-mineral thermometer. *Contributions to Mineralogy and Petrology*, **104**, 463–470.

Bigeleisen J., Perlman M.L. & Prosser H.C. (1952) Conversion of hydrogenic materials to hydrogen for isotopic analysis. *Analytical Chemistry*, **24**, 356–1357.

Bird M.I. & Chivas A.R. (1988) Stable-isotope evidence for low temperature kaolinitic weathering and post-formational hydrogen-isotope exchange in Permian kaolinites. *Chemical Geology (Isotope Geosciences)*, **72**, 249–265.

Bonhomme M., Thuizat R., Pinault Y., Clauer N., Wendling R. & Winkler R. (1975) *Méthode de datation potassium-argon. Appareillage et technique.* Technical report of the Centre de Géochimie de la Surface, Université Louis Pasteur Strasbourg, 53 pp.

Borthwick J. & Harmon R.S. (1982) A note regarding ClF_3 as an alternative to BrF_5 for oxygen isotope analysis. *Geochimica et Cosmochimica Acta*, **46**, 1665–1668.

Burley S.D. & Flisch M. (1989) K-Ar chronology and the origin of illite in Piper and Tartan fields, Outer Moray Firth, U.K. North Sea. *Clay Minerals*, **24**, 285–315.

Capuano R.M. (1992) The temperature dependence of hydrogen isotope fractionation between clay minerals and water: Evidence from a geopressured system. *Geochimica et Cosmochimica Acta*, **56**, 2547–2554.

Clauer N. (2006) Towards an isotopic modeling of the illitization process based on data of illite-type fundamental particles from mixed layered illite-smectite. *Clays and Clay Minerals*, **54**, 119–130.

Clauer N. & Chaudhuri S. (1995) *Clays in Crustal Environments. Isotope Dating and Tracing*. Springer Verlag, Heidelberg, New York, 359 pp.

Clauer N. & Chaudhuri S. (1996) Inter-basinal comparison of the diagenetic evolution of illite/smectite minerals in buried shales on the basis of K-Ar systematics. *Clays and Clay Minerals*, **44**, 818–824.

Clauer N. & Lerman A. (2009) A model for potassium gain and radiogenic argon loss during burial illitization based on analytical data. *46th Annual Meeting of the Clay Minerals Society*, Billings, MT, June 5–11, 2009, p. 91.

Clauer N., Chaudhuri S., Kralik M. & Bonnot-Courtois C. (1993) Effects of experimental leaching on Rb-Sr and K-Ar isotopic systems and REE contents of diagenetic illite. *Chemical Geology*, **103**, 1–16.

Clauer N., Środoń J., Franců J. & Šucha V. (1997) K-Ar dating of illite fundamental particles separated from illite/smectite. *Clay Minerals*, **32**, 181–196.

Clauer N., Rinckenbach T., Weber F., Sommer F., Chaudhuri S. & O'Neil J.R. (1999) Diagenetic evolution of clay minerals in oil-bearing Neogene sandstones and associated shales from Mahakam Delta Basin (Kalimantan, Indonesia). *American Association of Petroleum Geologists Bulletin*, **83**, 62–87.

Clayton R.N. & Mayeda T.K. (1963) The use of bromine pentafluoride in the extraction of oxygen from oxides and silicates for isotopic analysis. *Geochimica et Cosmochimica Acta*, **27**, 43–52.

Deconinck J.F., Strasser A. & Debrabant P. (1988) Formation of illitic minerals at surface temperatures in Purbeckian sediments (Lower Barresian, Swiss and French Jura). *Clay Minerals*, **23**, 91–103.

Delgado A. & Reyes E. (1996) Oxygen and hydrogen isotope compositions in clay minerals: a potential single-mineral geothermometer. *Geochimica et Cosmochimica Acta*, **60**, 4285–4289.

Donnelly T., Waldron S., Tait A., Dougans J. & Bearhop S. (2000) Hydrogen isotope analysis of natural abundance and deuterium-enriched waters by reduction over chromium on-line to a dynamic dual inlet isotope-ratio mass spectrometer. *Rapid Communications in Mass Spectrometry*, **15**, 1297–1303.

Dunoyer de Segonzac G. (1970) The transformation of clay minerals during diagenesis and low-grade metamorphism: A review. *Sedimentology*, **15**, 281–346.

Eberl D.D., Nuesch R., Šucha V. & Tsipursky S. (1998a) Measurement of fundamental illite particle thickness by X-ray diffraction using PVP-10 intercalation. *Clays and Clay Minerals*, **46**, 89–97.

Eberl D.D., Drits V.Q. & Środoń J. (1998b) Deducing growth mechanisms for minerals from the shapes of crystal size distributions. *American Journal of Science*, **298**, 499–533.

Eberl D.D., Drits V.Q. & Środoń J. (2001) User's guide to GALOPER – a program for simulating the shapes of crystal size distributions – and associated programs. *U.S. Geological Survey Open-File Report* OF00-505, 44 pp.

Eberl D.D., Blum A.E. & Serravezza M. (2011) Anatomy of a metabentonite: Nucleation and growth of illite crystals and their coalescence into mixed-layer illite/smectite. *American Mineralogist*, **96**, 586–593.

Ehrenberg S.N. & Nadeau P.H. (1989) Formation of diagenetic illite in sandstones of the Garn Formation, Haltenbanken area, mid-Norwegian continental shelf. *Clay Minerals*, **24**, 233–253.

Elliott W.C., Aronson J.L., Matisoff G. & Gautier D.L. (1991) Kinetics of the smectite to illite transformation in the Denver Basin; Clay mineral, K-Ar data and mathematical model results. *American Association of Petroleum Geologists Bulletin*, **75**, 436–462.

Eslinger E.V. & Savin S.M. (1973) Oxygen isotope geothermometry of the burial metamorphic rocks of the Precambrian Belt Supergroup, Glacier National Park, Montana. *Geological Society of America Bulletin*, **84**, 2549–2560.

Essene E.J. & Peacor D.R. (1995) Clay mineral thermometry – a critical perspective. *Clays and Clay Minerals*, **43**, 540–553.

Fallick A.E., Macaulay C.I. & Haszeldine R.S. (1993) Implications of linearly correlated oxygen and hydrogen isotopic compositions for kaolinite and illite in the Magnus Sandstone, North Sea. *Clays and Clay Minerals*, **41**, 184–190.

Franců J., Muller P., Šucha V. & Zatkaliková V. (1990) Organic matter and clay minerals as indicators of thermal history in the Transcarpathian Depression (East Slovakian Neogene Basin) and the Vienna Basin. *Geologica Carpathica*, **41**, 535–546.

Girard J.P. & Barnes D.A. (1995) Illitization and paleothermal regimes in the Middle Ordovician St Peter Sandstone, Central Michigan Basin, United States: K-Ar, oxygen isotopes, and fluid inclusion data. *American Association of Petroleum Geologists Bulletin*, **79**, 49–69.

Glasmann J.R., Larter S., Briedis N.A. & Lundegard P.D. (1989a) Shale diagenesis in the Bergen area, North Sea. *Clays and Clay Minerals*, **37**, 97–112.

Glasmann J.R., Lundegard P.D., Clark R.A., Penny B.K. & Collins I.D. (1989b) Geochemical evidence for the history of diagenesis and fluid migration: Brent sandstone, Heather Field, North Sea. *Clay Minerals*, **24**, 255–284.

Graham C.M. & Sheppard S.M.F. (1980) Experimental hydrogen isotope studies, II. Fractionations in the systems epidote–NaCl–H_2O, epidote–$CaCl_2$–H_2O and epidote–seawater, and the hydrogen isotope composition of natural epidotes. *Earth and Planetary Science Letters*, **49**, 237–251.

Hay R.L., Guldman S.G., Matthews J.C., Lander R.H., Duffin M.E. & Kyser T.K. (1991) Clay mineral diagenesis in core KM-3 of Searles Lake, California. *Clays and Clay Minerals*, **39**, 84–96.

Honty M., Uhlík P., Šucha V., Čaplovičová M., Franců J., Clauer N. & Biroň A. (2004) Smectite to illite alteration in salt-bearing bentonites (the East Slovak Basin). *Clays and Clay Minerals*, **52**, 533–551.

Honty M., Clauer N. & Šucha V. (2008) Rare-earth element systematics of mixed-layered illite-smectite from sedimentary and hydrothermal environments of the Western Carpathians (Slovakia). *Chemical Geology*, **249**, 167–190.

Horita J., Wesolowski D.J. & Cole D.R. (1993a) The activity-composition relationship of oxygen and

https://doi.org/10.1180/claymin.2014.049.2.07 Published online by Cambridge University Press

hydrogen isotopes in aqueous salt solutions: I Vapor-liquid equilibration of single salt solutions from 50 to 100ºC. *Geochimica et Cosmochimica Acta*, **57**, 2797–2817.

Horita J., Cole D.R. & Wesolowski D.J. (1993b) The activity-composition relationship of oxygen and hydrogen isotopes in salt solutions: II Vapor-liquid equilibration of mixed salt solutions from 50 to 100ºC and geochemical implications. *Geochimica et Cosmochimica Acta*, **57**, 4703–4711.

Hower J., Eslinger E.V., Hower M. & Perry E.A. (1976) Mechanism of burial metamorphism of argillaceous sediments: 1. Mineralogical and chemical evidence. *Geological Society of America Bulletin*, **87**, 725–737.

Jackson M.L. (1975) *Soil Chemical Analysis – Advanced Course.* Madison, Wisconsin, 386 pp.

Jennings S. & Thompson G.R. (1986) Diagenesis of Plio-Pleistocene sediments of the Colorado River delta, southern California. *Journal of Sedimentary Petrology*, **56**, 89–98.

Kolata D.R., Huff W.D. & Berström S.M. (1996) Ordovician K-bentonites of eastern North America. *Geological Society of America, Special Paper* 313, 84 pp.

Kováč M., Kováč P., Marko F., Karoli S. & Janočko J. (1995) The East Slovakian Basin – a complex back arc basin. *Tectonophysics*, **252**, 453–466.

Kováč M., Bielik M., Lexa J., Pereszlényi M., Šefara J., Túnyi I. & Vass D. (1997) The Western Carpathian intramontane basins. Pp. 43–64 in: *Geological Evolution of the Western Carpathians* (P. Grecula, D. Hovorka & M. Putiš, editors). Geological Survey of Slovak Republic, Bratislava.

Král M., Lizoň I. & Jančí J. (1985) Geothermal Research of Slovakia. *Manuscript, Geofond*, Bratislava, Open File Report, 1–116 (in Slovak).

Kübler B. (1997) Concomitant alteration of clay minerals and organic matter during burial diagenesis. Pp. 327–362 in: *Soils and Sediments* (H. Paquet & N. Clauer, editors). Springer Verlag, Heidelberg, New York.

Lee M. (1984) Diagenesis of the Permian Rotliegendes Sandstone, North Sea: K/Ar, O^{18}/O^{16} and petrologic evidence. Ph.D. Thesis, Case Western Reserve University, Cleveland, OH.

Lerman A., Ray B.M. & Clauer N. (2007) Radioactive production and diffusional loss of radiogenic ^{40}Ar in clays in relation to its flux to the atmosphere. *Chemical Geology*, **243**, 205–224.

Longstaffe F.J. & Ayalon A. (1990) Hydrogen-isotope geochemistry of diagenetic clay minerals from Cretaceous sandstones, Alberta, Canada: Evidence for exchange. *Applied Geochemistry*, **5**, 657–668.

Macaulay C.I., Fallick A.E., Haszeldine R.S. & Graham C.M. (2000) Methods of laser-based stable isotope measurement applied to diagenetic cements and hydrocarbon reservoir quality. *Clay Minerals*, **35**, 317–326.

McCarty D.K., Sakarov B.A. & Drits V.A. (2008) Early clay diagenesis in Gulf Coast sediments: New insights from XRD profile modeling. *Clays and Clay Minerals*, **56**, 359–379.

McCarty D.K., Sakharov B.A. & Drits V.A. (2009) New insights into smectite illitization: A zoned K-bentonite revisited. *American Mineralogist*, **94**, 1653–1671.

Magyar J. & Očovský J. (1981) Final report on the investigation of the deep structural borehole Pavlovce 1. *Open File Report, Nafta-Gbely, Michalovce*, 23 pp. (in Slovak).

Michaliček M. (1965) Prispevek k hydrogeochemii a geologii hlubinnch vod Trebisoske niziny. *Geologicke prace, Zpravy*, **35**, 167–185 (in Czech).

Michaliček M. (1970) K puvodu chloridosodnych solanek v miocenu trebisovske niziny. *Sbornik geologickych ved, rada HIG*, **7**, 107–159 (in Czech).

Morton J.P. (1985) Rb-Sr evidence for punctuated illite/smectite diagenesis in the Oligocene Frio Formation, Texas Gulf Coast. *Geological Society of America Bulletin*, **96**, 114–122.

Mossmann J.R. (1991) K-Ar dating of authigenic illite-smectite clay material: application to complex mixtures of mixed-layer assemblages. *Clay Minerals*, **26**, 189–198.

Nadeau P.H., Wilson M.J., McHardy W.J. & Tait J.M. (1984) Interstratified clays as fundamental particles. *Science*, **225**, 923–925.

Nier A.O. (1950) A redetermination of the relative abundances of the isotopes of carbon, nitrogen, oxygen, argon and potassium. *Physical Review*, **77**, 789–793.

Odin G. S. & 35 collaborators (1982) Interlaboratory standards for dating purposes. Pp. 123–148 in: *Numerical Dating in Stratigraphy, Part 1* (G.S. Odin, editor). John Wiley & Sons, Chichester.

O'Neil J.R. (1992) Stable isotope exchange in fluid-mineral systems: Old problems, new solutions. Pp. 861–864 in: *Water-Rock Interaction WRI-7* (Y.K. Kharaka & A.S. Maest, editors). Balkema, Rotterdam.

O'Neil J.R. & Truesdell A.H. (1991) Oxygen isotope fractionation studies of solute-water interactions. Pp. 17–25 in: *A Tribute to Samuel Epstein* (H.P. Taylor Jr., J.R. O'Neil & I. Kaplan, editors). *Geochemical Society, Special Publication*, **3**.

Peacor D.R. (1992) Diagenesis and low-grade metamorphism of shales and slates. Pp. 335–380 in: *Minerals and Reactions at Atomic Scale: Transmission Electron Microscopy* (P.R. Buseck, editor). *Reviews in Mineralogy*, **27**, Mineralogical Society of America.

Poelchau H.S., Baker D.R., Hantschel T., Horsfield B. & Wygrala B. (1997) Basin simulation and the design

https://doi.org/10.1180/claymin.2014.049.2.07 Published online by Cambridge University Press

of the conceptual basin model. Pp. 5–70 in: *Petroleum and Basin Evolution* (D.H. Welte, B. Horsfield & D.R. Baker, editor). Springer Verlag, Berlin, Heidelberg, New York.

Royden L.H. (1993) The tectonic expression of slab pull at continental convergent boundaries. *Tectonics*, **12**, 303–325.

Rudinec R. (1990) Vertical distribution of Neogene sediments in the Transcarpathian depression. *Mineralogica Slovaca*, **22**, 393–397.

Savin S.M. & Lee M. (1988) Isotopic studies of phyllosilicates. *Reviews in Mineralogy*, **19**, Mineralogical Society of America, 189–223.

Sheppard S.M.F. (1986) Characterisation and isotopic variations in natural waters. *Reviews in Mineralogy*, **16**, Mineralogical Society of America, 165–183.

Sheppard S.M.F. & Gilg H.A. (1996) Stable isotope geochemistry of clay minerals. *Clay Minerals*, **31**, 1–24.

Singer A. & Stoffers P. (1980) Clay mineral diagenesis in two East African lake sediments. *Clay Minerals*, **15**, 291–307.

Soták J., Biroň A. & Spišiak J. (1993) The Penninic "pull-apart" dome in the pre-Neogene basement of the Transcarpathian depression (Eastern Slovakia). *Geologica Carpathica*, **44**, 11–16.

Środoń J. (1980) Precise identification of illite/smectite interstratifications by X-ray powder diffraction. *Clays and Clay Minerals*, **28**, 401–411.

Środoń J. (1984) X-ray identification of illitic materials. *Clays and Clay Minerals*, **32**, 337–349.

Środoń J. (1999) Extracting K-Ar ages from shales: a theoretical test. *Clay Minerals*, **33**, 375–378.

Środoń J. & Eberl D.D. (1984) Illite. Pp. 495–544 in: *Micas* (S.W. Bailey, editor). *Reviews in Mineralogy*, **13**. Mineralogical Society of America.

Środoń J., Elsass F., McHardy W.J. & Morgan D.J. (1992) Chemistry of illite/smectite inferred from TEM measurements of fundamental particles. *Clay Minerals*, **27**, 137–158.

Środoń J., Eberl D.D. & Drits V.A. (2000) Evolution of fundamental-particle size during illitization of smectite and implications for reaction mechanism. *Clays and Clay Minerals*, **48**, 446–458.

Środoń J., Clauer N. & Eberl D.D. (2002) Interpretation of K-Ar dates of illitic clays from sedimentary rocks aided by modeling. *American Mineralogist*, **87**, 1528–1535.

Środoń J., Kotarba M., Biroň A., Such P., Clauer N. & Wojtowicz A. (2006) Diagenetic history of the Podhale-Orava Basin and the underlying Tatra sedimentary structural units (Western Carpathians): Evidence from XRD and K-Ar of illite-smectite. *Clay Minerals*, **41**, 751–774.

Steiger R. & Jäger E. (1977) Subcommission on Geochronology: Convention on the use of decay constants in geo- and cosmochronology. *Earth and Planetary Science Letters*, **36**, 359–362.

Šucha V., Kraus I., Gerthofferová H., Peteš J. & Sereková M. (1993) Smectite to illite conversion in bentonites and shales of the East Slovak Basin. *Clay Minerals*, **28**, 243–253.

Sweeney J.J. & Burnham A.K. (1990) Evaluation of a simple model of vitrinite reflectance based on chemical kinetics. *American Association of Petroleum Geologists Bulletin*, **74**, 1559–1570.

Szczerba M. & Środoń J. (2009) Extraction of diagenetic and detrital ages and of the $^{40}K_{detrital}/^{40}K_{diagenetic}$ ratio from K-Ar dates of clay fractions. *Clays and Clay Minerals*, **57**, 93–103.

Tomek Č. & Hall J. (1993) Subducted continental margin imaged in the Carpathians of Czechoslovakia. *Geology*, **21**, 535–538.

Turner C.E. & Fishman N.S. (1991) Jurassic lake T'oo'dechi': a large alkaline, saline lake, Morrison formation, eastern Colorado Plateau. *Geological Society of America Bulletin*, **103**, 538–558.

Vaas, D., Kováč, M., Konečný, V. & Lexa, J. (1988) Molasse basins and volcanic activity in West Carpathian Neogene – its evolution and geodynamic character. *Geologica Carpathica*, **39**, 539–562.

Velde B. (1985) Clay Minerals: a Physico-Chemical Explanation of their Occurrence. Developments in Sedimentology, **40**. Elsevier, Amsterdam, 426 pp.

Whitney G. & Northrop H.R. (1988) Experimental investigation of the smectite to illite reaction: dual reaction mechanisms and oxygen-isotope systematics. *American Mineralogist*, **73**, 77–90.

https://doi.org/10.1180/claymin.2014.049.2.07 Published online by Cambridge University Press